

Feedforward Wind Turbine Control Design Using LIDAR

Mengling Wang

Industrial Control Centre,
Department of Electronic and Electrical Engineering,
University of Strathclyde,
204 George Street,
Glasgow G1 1XW

Thesis submitted to the
University of Strathclyde
for the degree of
Master of Philosophy

August 2015

This thesis is the result of the author's original research. It has been composed by the author and has not been previously submitted for examination which has led to the award of a degree.

The copyright of this thesis belongs to the author under the terms of the United Kingdom Copyright Acts as qualified by University of Strathclyde Regulation 3.51. Due acknowledgement must always be made of the use of any material contained in, or derived from, this thesis.

Acknowledgements

First of all, I would like to thank my supervisor Professor Bill Leithead to give me an opportunity to study in the United Kingdom. I give many thanks to my second supervisor Dr Hong Yue for her patient guidance for my project and time spent on correcting my academic writing.

I appreciate Dr Sung-Ho Hur and Yi Han for the time they spent for answering my questions and useful conversations on how to solve problems, also Dr Adam Stock who provides Supergen wind turbine models.

I give many thanks to my parents for their love and never ending support, my friend Xin Li for her everlasting friendship and support. Finally, I want to thank Jesus for His love and grace during my time in Glasgow.

To my parents, Yijin Wang and Youlin Lu

Abstract

Recent development in Light Detection And Ranging (LIDAR) systems, which can provide measurements of the wind upstream of wind turbine, opens a new area of research in wind turbine control. The main objective of this research project is to explore the feasibility of using LIDAR and feedforward control strategy to improve wind turbine operation.

In this study, a model-inverse feedforward control strategy is employed for the pitch control. LIDAR measured wind speed is fed into the feedforward controller. LIDAR measurements and the wind speed approaching the turbine are simulated using software package GH Bladed. The transfer function representing the evolution of wind speed is developed. The feedforward controller design is based on the Supergen 5MW linear wind turbine models and the transfer function. It is augmented to the predesigned feedback pitch controller.

The system outputs before and after the addition of the feedforward controller are compared. The whole system is operated in Matlab/Simulink environment. Simulation results show that combining the baseline feedback control with feedforward control is able to reduce the blade and tower loads.

Contents

ACKNOWLEDGEMENTS	I
ABSTRACT	III
CONTENTS	IV
LIST OF FIGURES.....	VII
LIST OF TABLES	X
NOMENCLATURE	XI
1 INTRODUCTION.....	1
1.1 BACKGROUND.....	1
1.2 OBJECTIVES	3
1.3 THESIS OUTLINE	3
1.4 PUBLICATIONS	4
2 OVERVIEW OF WIND TURBINE SYSTEMS AND THE ASSOCIATED CONTROLLER.....	5
2.1 INTRODUCTION TO WIND TURBINES	5
2.1.1 The Structure of a Wind Turbine	5
2.1.2 Wind Turbine Modelling Software	7

Contents

2.2 OVERVIEW OF WIND TURBINE CONTROL SYSTEM DESIGN	8
2.2.1 Wind Speed Model	8
2.2.2 Wind Turbine Feedback Controller	9
2.2.3 Controller to Alleviate Unbalanced Rotor Loads	10
2.3 SUPERGEN 5MW WIND TURBINE MODEL	13
2.3.1 Wind Turbine Modelling	13
2.3.2 Supergen Baseline Controller	17
3 LIDAR TECHNIQUES	19
3.1 OVERVIEW OF LIDAR TECHNIQUES	19
3.2 LIDAR MEASUREMENT THEORY	23
3.3 LIDAR FOR WIND TURBINE CONTROL	24
4 DESIGN OF FEEDFORWARD CONTROLLER.....	28
4.1 THE LIDAR PREVIEW	30
4.2 THE FEEDFORWARD CONTROLLER	31
4.2.1 Cross Correlation Study	33
4.2.2 Wind Speed Simulation	34
4.2.3 Cross Correlation and Cross Spectrum	39
4.2.4 Wind Turbine Model Linearisation	42
4.3 SIMULATION RESULTS	46
4.3.1 Simulation Results for Feedforward Controller I.....	46
4.3.2 Simulation Results for Feedforward Controller II.....	52
5 CONCLUSIONS AND FUTURE WORK	62

Contents

REFERENCES	64
APPENDIX A 5MW SUPERGEN EXEMPLAR WIND TURBINE	
PARAMETERS.....	67
APPENDIX B 5MW WIND TURBINE LINEAR MODEL	70
B.1 5MW WIND TURBINE STATE-SPACE MODEL.....	70
B.1.1 Linear Model I.....	70
<i>B.1.1.1 When the pitch angle is the input and the generator speed is the output</i>	<i>70</i>
<i>B.1.1.2 When the wind speed is the input and the generator speed is the output</i>	<i>70</i>
B.1.2 Linear Model II.....	73
<i>B.1.2.1 When the pitch angle is the input and the generator speed is the output</i>	<i>73</i>
<i>B.1.2.2 When the wind speed is the input and the generator speed is the output</i>	<i>75</i>
B.2 5MW WIND TURBINE TRANSFER FUNCTION MODEL	77
B.2.1 Transfer Functions for Wind Turbine Model I	77
B.2.2 Transfer Functions for Wind Turbine Mode II	78
APPENDIX C MATLAB CODE FOR THE PROJECT	79
C.1 CODE FOR CROSS CORRELATION.....	79
C.2 CODE FOR POWER SPECTRUM	81
C.3 CODE FOR CROSS POWER SPECTRUM	83
C.4 WIND TURBINE CONTROL SYSTEM SIMULINK MODEL	85

List of Figures

Figure 1.1	Cumulative capacity installed globally 1996-2013 [2].....	2
Figure 1.2	Evolution of standard rotor diameters [4]	2
Figure 2.1	The major components of a wind turbine [6]	5
Figure 2.2	Individual pitch control loop using d-q axis transformation	12
Figure 2.3	The structure of the IBC [26]	12
Figure 2.4	Dynamic model of the wind turbine.....	13
Figure 2.5	Drive-train model [16]	16
Figure 2.6	Ideal operating strategy of the Supergen 5MW wind turbine	17
Figure 3.1	Generic bistatic LIDAR system [33].....	22
Figure 3.2	Coordinate system for LIDAR measurement [35]	23
Figure 3.3	Coordinate system for LIDAR measurement with scan radius.....	24
Figure 4.1	Block diagram of feedback baseline control [43].....	28
Figure 4.2	Combined feedback and feedforward control	29
Figure 4.3	Scope of simulated LIDAR measurements [11]	30
Figure 4.4	Feedforward control scheme	31
Figure 4.5	The Relationship between v_L and v_T	32
Figure 4.6	Modified feedforward control scheme	32
Figure 4.7	3D wind volume simulated by Bladed	34
Figure 4.8	Distribution of v_T and $v_{Li}(t_{Li}, x_{Li})(i = 1, \dots, 6)$	36
Figure 4.9	Schematics of wind speed sampling in Bladed.....	37
Figure 4.10	Modified distribution of the turbine wind speed and LIDAR measurements	38
Figure 4.11	Lateral components of v_T , v_{L1} , v_{L2} and v_{L3}	38
Figure 4.12	Cross correlation between the turbine wind speed v_T and LIDAR measurements	39

List of Figures

Figure 4.13	Zoom-in figure of cross correlation for distance axis between -100m to 100m	39
Figure 4.14	Cross spectrum of the turbine wind speed and LIDAR measurements	40
Figure 4.15	Auto spectrum of LIDAR measurements.....	41
Figure 4.16	Comparison of simulated model output and measured model output.....	41
Figure 4.17	LIDAR measurement and turbine wind speed for model I	47
Figure 4.18	Comparison of the blade pitch angle before and after the addition of the feedforward controllers with k_{FF1} and k_{FF2}	48
Figure 4.19	Comparison of the generator speed before and after the addition of the feedforward controllers with k_{FF1} and k_{FF2}	48
Figure 4.20	Comparison of the generator power before and after the addition of the feedforward controllers with k_{FF1} and k_{FF2}	49
Figure 4.21	Comparison of the tower acceleration before and after the addition of the feedforward controllers with k_{FF1} and k_{FF2}	49
Figure 4.22	Comparisons of In-plane and Out-of-plane blade torques before and after the addition of the feedforward controller with k_{FF1}	51
Figure 4.23	Spectra of the pitch demand for wind speed at 12m/s	51
Figure 4.24	Spectra of the tower acceleration for wind speed at 12m/s	52
Figure 4.25	LIDAR measurement and turbine wind speed for controller II.....	53
Figure 4.26	Comparison of the blade pitch angle between baseline controller and feedforward controllers with k_{FF3} and k_{FF4}	53
Figure 4.27	Comparison of the tower acceleration between baseline controller and feedforward controllers with k_{FF3} and k_{FF4}	54
Figure 4.28	Comparison of the generator speed between baseline controller and feedforward controllers with k_{FF3} and k_{FF4}	55
Figure 4.29	Comparison of the generator power between baseline controller and feedforward controllers with k_{FF3} and k_{FF4}	55

List of Figures

Figure 4.30:	Comparisons of In-plane and Out-of-plane blade torques before and after the addition of the feedforward controller with k_{FF3}	56
Figure 4.31	Spectra of the pitch demand for 16m/s wind speed	57
Figure 4.32	Spectra of the tower acceleration for 16m/s wind speed	57
Figure 4.33	Open-loop Bode plot from Wind Speed to Generator Speed for 16m/s	58
Figure 4.34	Open-loop Bode plot from Wind Speed to Hub Torque for 16m/s ..	59
Figure 4.35	Open-loop Bode plot from Wind Speed to Tower Acceleration for 16m/s	59
Figure 4.36	Open-loop Bode plot from Pitch Demand to Generator Speed for 16m/s	60
Figure 4.37	Open-loop Bode plot from Pitch Demand to Tower Acceleration for 16m/s	60
Figure 4.38	Open-loop Bode plot from Pitch Demand to Hub Torque for 16m/s	61
Figure C.1	Simulink model of the whole control system.....	85
Figure C.2	Wind turbine Simulink model.....	86
Figure C.3	Part 1 of the baseline controller.....	87
Figure C.4	Part 2 of the baseline controller.....	88
Figure C.5	Feedforward control loop.....	89

List of Tables

Table 4.1	Parameters of the turbine	35
Table 4.2	Characterises of turbulence	35
Table 4.3	Characterises of 3D turbulence	35

Nomenclature

T_f	Aerodynamic torque
U	Wind speed
Ω	Rotor speed
β	Pitch angle
λ	Tip speed ratio
R	Rotor radius
ρ	Air density
x_a, x_b and x_c	Directions with phase angle of 0, 120 and 240 degree
x_d and x_q	Vertical and lateral directions
$S_{VK}(\omega)$	The Von Karman spectrum
σ_v	Standard deviation of wind speed
l_u	Turbulence length scale factor
ω	White Gaussian noise
\bar{U}	Mean wind speed
S_D	The Dryden spectrum
k_1 and a	Parameters selected to best fit the Dryden spectrum to the Von Karma spectrum
v_{pw}	Point wind
$v_{effective}$	Effective wind
σ and a'	Parameters of the spatial filter for effective wind speed
γ	Turbulent wind speed decay factor
\hat{v}	Time averaging mean wind speed
k_2 and b	Parameters of the 1 st order time-averaging wind speed filter
M_1, M_2 and M_3	Measured blade loads

Nomenclature

β_1, β_2 and β_3	Pitch demands
I_1	Rotor inertia
I_2	Generator inertia
N	Gearbox ratio
K_1	Low-speed shaft stiffness
K_2	High-speed shaft stiffness
γ_1	Low-speed shaft external damping coefficient
γ_2	High-speed shaft external damping coefficient
γ_1^*	Low-speed shaft internal damping coefficient
γ_2^*	High-speed shaft internal damping coefficient
δv	Change in the light's frequency via the Doppler shift
V_{LOS}	Component of target speed along the line of sight
c	Speed of light
ν'	Laser frequency
λ'	Laser wavelength
σ'	Standard deviation of wind speed variations about the mean wind speed
x, y and z	Three axis of coordinate system
u, v and w	Three components of wind speed
v_{dec}	Detected radial wind velocity
d	Preview distance
r	Scan radius
FB	Feedback controller
FF	Feedforward controller
β_{FF}	Pitch angle of feedforward controller
β_{FB}	Pitch angle of feedback controller
β_c	Total pitch angle command
v_T	Turbine wind speed
v_L	LIDAR measured wind speed

Nomenclature

S_{LT}	Cross spectrum between the LIDAR measured wind speed and the turbine wind speed
S_{LL}	Auto spectrum of LIDAR measured wind speeds
ω_e	Generator speed error
β_0, ω_0 and U_0	Specific operating point
ω_g	Generator speed
ω_{g_rated}	Rated generator speed
ω_{g_actual}	Actual generator speed
$P_{\omega_e\beta_c}$	Turbine transfer function from collective blade pitch error to generator speed error
$P_{\omega_e v_t}$	Turbine transfer function from deviation from nominal wind speed to generator speed error
k	Wave-number
f	Cut-off frequency

Abbreviations List

LIDAR	Light Detection And Ranging
BEM	Blade Element Momentum theory
PID	Proportional Integral Derivative
CFD	Computational Fluid Dynamics
IPC	Individual Pitch Control
d-q	direct-quadrature
IBC	Individual Blade Control
LDA	Laser Doppler Anemometry
LDV	Laser Doppler Velocimetry
PIV	Particle Imaging Velocimetry

Nomenclature

DGV	Doppler Global Velocimetry
MPC	Model Predictive Control
DAC	Disturbance Accommodating Controller
SODAR	SOund Detection And Ranging
ABL	Atmospheric Boundary Layer

Chapter 1

Introduction

1.1 Background

Energy is the important material basis for human survival and development. However, there is a big concern over the shortages of energy supplies in recent years [1]. On one side, our need for energy is increasing rapidly, and on the other side, conventional energy sources such as coal, oil and gas are limited and bring damage to the earth's atmosphere. Recently in Asia, especially China, smog has become a hot spot, which is the result of coal and petrol consumption.

The most feasible method to reduce dependence on conventional energy is to develop renewable energy technologies. Types of renewable energy technologies include solar energy, geothermal energy, wind energy, ocean energy, hydropower, etc. Among them, wind energy is the world's fastest growing renewable energy type and makes a significant contribution to the UK's energy needs. According to Renewable UK's latest annual report, 9.3% of the UK's total electricity supply in 2014 was provided by wind energy [2].

The rapid growth of wind power not only occurs in the UK, but also in many other countries around the world. The most recent statistics from World Wind Energy Association illustrate that the worldwide wind capacity has reached more than

Chapter 1. Introduction

350GW, with annual growth rate of 13.5% in 2014 [3]. The global wind power cumulative capacity installed from 1996 to 2013 is shown in Figure 1.1.

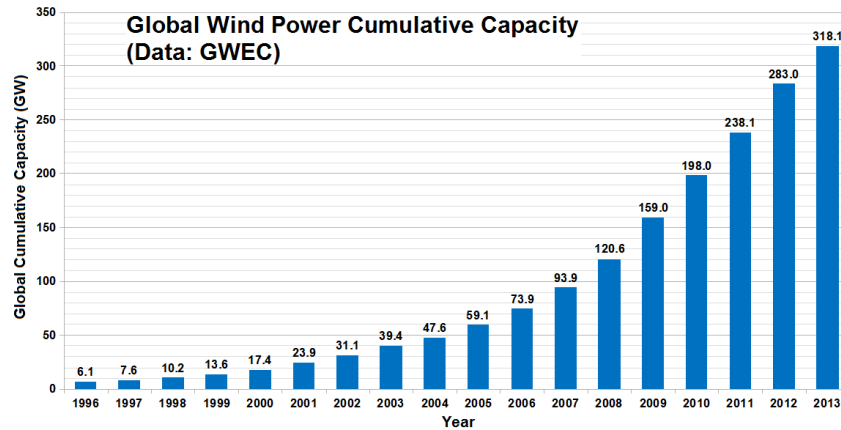


Figure 1.1: Cumulative capacity installed globally 1996-2013 [2]

At the same time, the average size of wind turbines is growing rapidly as shown in Figure 1.2. The rotor diameter has been increased from 15m in 1985 to more than 150m today.

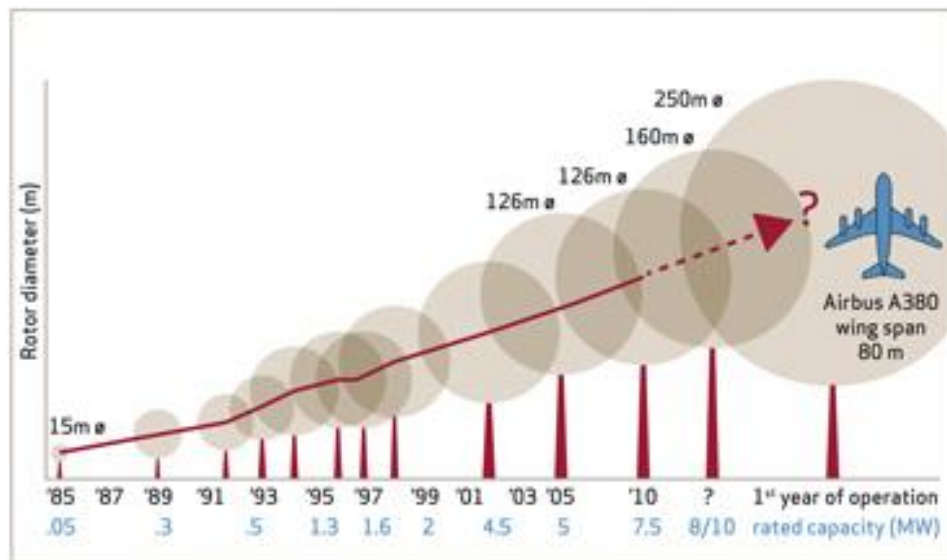


Figure 1.2: Evolution of standard rotor diameters [4]

Low and stable cost is very important for the development of wind power. The growth in size and capability brings more challenging problems to the maintenance

Chapter 1. Introduction

system of wind turbines, which hence increases the cost of wind power generation. Advanced controllers with high performance and reliability are able to enhance the efficiency of the power generation and contribute to the wind energy cost reduction [5].

In recent years, motivated by higher expectation of wind turbine performance, increasing attention is being paid to advanced measurement technologies. LIDAR (Light Detection And Ranging) is able to provide preview information of wind disturbances at various distances in front of wind turbines. With the help of LIDAR measurements, advanced control strategies can be introduced into the wind energy to alleviate wind turbine structural loads.

1.2 Objectives

The objective of the thesis is to investigate the performance improvement in load reduction and/or energy capture by introducing a LIDAR-based pitch control strategy in horizontal axis wind turbines. To achieve this objective, a feedforward control loop is added to the conventional feedback pitch controller. The research compares the performance of the wind turbine control system after and before the addition of the feedforward controller.

1.3 Thesis Outline

The thesis is organized as follows:

Chapter 1 includes a brief report of wind energy development, the motivation and organisation of this thesis.

In Chapter 2, the basic information of wind turbine models is given and the Supergen

Chapter 1. Introduction

5MW wind turbine model is described.

In Chapter 3, the primary types of remote sensing techniques are introduced and the principle of coherence LIDAR is explained. Some control strategies using LIDAR measurements are also discussed in this Chapter.

In Chapter 4, both LIDAR measurements and turbine wind speed are simulated using software package GH Bladed. The transfer function representing the evolution of wind speed is developed and included in the feedforward controller design. Feedforward controllers are developed based on linear Supergen wind turbine models. At last, the system outputs before and after the addition of the feedforward controller are compared.

Finally in Chapter 5, the conclusions are presented with some discussion on future work.

1.4 Publications

The outcomes of this thesis resulted in the following publications:

1. Mengling Wang, Hong Yue, Jie Bao, William. E. Leithead, "LIDAR-based Wind Speed Modelling and Control System Design", Proceedings of the 21st International Conference on Automation & Computing, 11-12 September 2015, Glasgow , UK
2. Jie Bao, Mengling Wang, Hong Yue, William Leithead, "Pseudo-LIDAR Data Analysis and Feed-forward Wind Turbine Control Design", International Symposium on Advanced Control of Chemical Processes, 7-10 June 2015, Whistler, British Columbia, Canada

Chapter 2

Overview of Wind Turbine Systems and the Associated Controller

2.1 Introduction to Wind Turbines

2.1.1 The Structure of a Wind Turbine

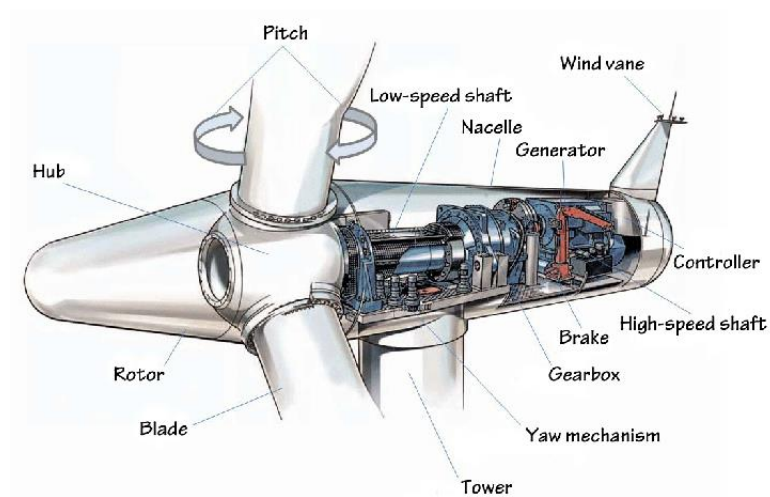


Figure 2.1: The major components of a wind turbine [6]

A wind turbine contains the following components:

Wind turbine foundation

Depending on the geotechnical conditions and the methods developed to resist overturning forces, various types of foundation are adopted for engineering purposes [7].

Rotor and blades

The rotor for a typical utility-scale wind turbine consists of two or three blades, a hub and a spinner. The blades are bolted onto the hub, with a pitch mechanism interposed to allow the blade to rotate about its axis. The blade profile is similar to that of an aeroplane wing. They use same principle of lift: on the lower side of the wing the passing air generates higher pressure, while the upper side generates a pull. The pressure difference causes the rotor to move forwards and convert wind energy into rotary mechanical movement.

A wind turbine may have one, two or three blades. Currently, the three-blade, horizontal axis turbine dominates the market. Compared with wind turbines with one or two blades, the three-blade turbine is more efficient and has less noise. However, it increases gearbox and transmission cost.

The rotor blades are made of laminated materials, such as balsa wood, carbon fibre, metal and fibreglass. Fibreglass is lightweight, strong, and inexpensive. It has good fatigue characteristics and is widely used in modern large wind turbines.

Nacelle

The nacelle of a wind turbine is the box-like component that sits atop the tower and is connected to the rotor. It contains the majority of the components of the wind turbine, such as the low-speed shaft, the high-speed shaft, the gearbox, etc.

Electronic equipment

This part includes generator, control box, converter, and various sensors, etc.

Other components

In addition to the main components, a wind turbine also contains anemometer, components for cooling, heating and lightning protection, as well as lifting gear and fire extinguishing equipment.

2.1.2 Wind Turbine Modelling Software

In order to support wind power industries with state-of-the-art analysis capabilities, some computer-aided tools are developed to simulate the behaviour of wind turbines in different ways. They can be used to model the effects of turbulence, structural dynamics, drive-train response, control systems, and loading. There are mainly two institutions developing wind power software packages: The National Wind Technology Centre (NWTC) located at the national renewable energy laboratory in the United States and Garrad Hassan & Partners Ltd, a British company based in Bristol, England.

NWTC computer-aided engineering tools [8]

TurbSim: This tool computes full-field stochastic wind realizations. Inputs are the desired wind profile and turbulence characteristics. It includes IEC and site-specific turbulence models, with an option to generate coherent structures.

FAST: This software package computes structural-dynamic and control-system responses as part of the aero-hydro-servo-elastic solution. The control system modelling is through subroutines, DLLs, or Simulink with MATLAB. It has nonlinear time domain solution for loads analysis, pre-processor for building turbine models in MSC.ADAMS, linearisation procedure for controls and stability analysis.

Chapter 2. Overview of Wind Turbine and Controller

GH Bladed

Bladed has been extensively validated against measured data from a wide range of wind turbines. It enables users to conduct the full range of performance and loading calculations. With a Windows-based user interface, it supports calculations of combined wind and wave loading. In Bladed, a kind of formulation called multibody structural dynamics is utilized. It provides consistently reliable and accurate results and forms a solid foundation so that the structural model can be extended with features. In addition to the core module, a series of specialist modules are included in the software: steady state analysis, dynamic load simulations, analysis of loads and energy capture, batch processing, automated report generation, interaction with the electrical network, and model linearisation for control design [9].

2.2 Overview of Wind Turbine Control System Design

2.2.1 Wind Speed Model

Wind speed model is a significant part for the whole wind turbine control system. Some primary wind speed models are introduced in this section.

The TurbSim stochastic full-field inflow simulator has been developed by researchers in National Wind Technology Centre. It is able to provide realistic wind fields for the wind turbine model [10]. UpWind reference turbine is proposed in [11], in which the wind field is simulated by software AeroDyn. In [5], mean wind speed, turbulence, tower shadow, wind shear and rotational sampling are combined to represent wind field. The white noise filtered through a filter e.g. Kaimal spectrum is the turbulence. The rotational sampling model includes two filters, a low pass filter and an extra filter. For IEC 61400-1 wind turbine model, the turbulence, gust, etc. are given by equations

Chapter 2. Overview of Wind Turbine and Controller

[12, 13]. In [14] and [15], Kalman estimator is used to estimate the states of wind speed model. The research group in University of Strathclyde proposes effective wind speed model [16, 17], [18], which will be illustrated in section 2.3.

2.2.2 Wind Turbine Feedback Controller

The wind turbine feedback controller can initially be thought of having two controllers: an above rated controller that acts on pitch and a below rated controller that acts on torque [4]. A switch is used to bridge the two controllers. The general design objectives for controllers are to maximise power capture below rated and to regulate the power above rated. In this study, only the design of pitch controller operating in above rated wind speed is discussed.

PID approach is common and effective for wind turbine pitch controller design. In [19], PID parameters K_p and K_i have gain-scheduling factors, which enable the two parameters vary with the pitch angle. The results suggest that the actual pitch angle is close to the value calculated from operation control strategy and the generator speed stays at the rated value. However, saturation on the pitch controller output is not included in the design. Further improvement of the performance of the controller is achieved when the saturation and rate limitation are added to the output of the pitch controller to restrict the action of pitch actuators [20]. In [12], a second order low pass Butterworth filter is added to the rotor speed signal. Simulation studies indicate that the low frequency disturbance in the wind is suppressed by the controller with bandwidth of 1 rad/s and damping of 0.707.

2.2.3 Controller to Alleviate Unbalanced Rotor Loads

The rapid increase in wind turbine size leads to greater demands on the wind turbine control system e.g. structural loads reduction. Some research is focused on the alleviation of asymmetric loads on the rotor.

When a turbine blade sweeps through the wind field, it experiences loads caused by the rotational sampling of the wind field. These $n\Omega$ loads are concentrated at integer multiples (n) of the rotor speed (Ω) and consist of both deterministic and stochastic components. The stochastic component largely arises from the turbulence of the wind. The deterministic loads largely arise from wind shear, tower shadow and blade imbalance. Since the wind field is continuously changing in time and over the swept area, each blade of the rotor experiences slightly different loads, which results in load imbalance across the rotor. These imbalances not only impact on the rotor but also on the rest of the wind turbine structure and the drive-train. The most significant components of these unbalanced loads are typically at 1Ω and 2Ω , which are called 1P and 2P loads.

Individual Pitch Control

Individual blade pitch control (IPC) has demonstrated great potential to alleviate rotor loads in above rated wind speed operation [21, 22]. It aims to reduce the asymmetric loads by varying the pitch angle of each blade individually in response to some suitable measurement such as blade bending moments. Improvements in sensor technology are now making this algorithm practically possible [22].

In previously reported approaches, individual pitch control is realised through the wind turbine central controller. The loads on each blade are measured, communicated to a controller which then determines the pitch angle demand for

Chapter 2. Overview of Wind Turbine and Controller

each blade using the measurements. The direct-quadrature (d-q) axis transformation is central to this procedure.

In [23], d-q axis transformation is applied on IPC for wind turbines. The transformation is originally used in the three-phase electrical machine theory. It is essentially the co-ordinate system transformation from the three-vector, $[x_a \ x_b \ x_c]^T$, to the two-vector, $[x_d \ x_q]^T$, such that

$$\begin{bmatrix} x_d \\ x_q \end{bmatrix} = \sqrt{\frac{2}{3}} \cdot \begin{bmatrix} \cos \psi & \cos(\psi - \frac{2\pi}{3}) & \cos(\psi + \frac{2\pi}{3}) \\ -\sin \psi & -\sin(\psi - \frac{2\pi}{3}) & -\sin(\psi + \frac{2\pi}{3}) \end{bmatrix} \begin{bmatrix} x_a \\ x_b \\ x_c \end{bmatrix} \quad (1)$$

In electrical machine theory, a-, b- and c- axes represent directions with phase angle of 0° , 120° and 240° . d- and q- axes represent the vertical and lateral directions. The angle ψ , parameterising the transformation, is the azimuth angle.

IPC is demonstrated briefly in Figure 2.2. When d-q axis transformation is used for IPC, measurements such as blade root bending moments are transformed into the d- and q- axes using equation (1). Therefore, the blade bending moment measurements in a rotating frame can then be expressed as load measurements in a fixed frame. Pitch demands are calculated based on the measurements in the d- and q- axes and they can be inversely transformed to be combined with collective pitch demand from the central controller. Test results indicate noticeable reductions in 1P and 2P loads in the blades (10-25%) and the yaw bearing (20-40%) [21-23].

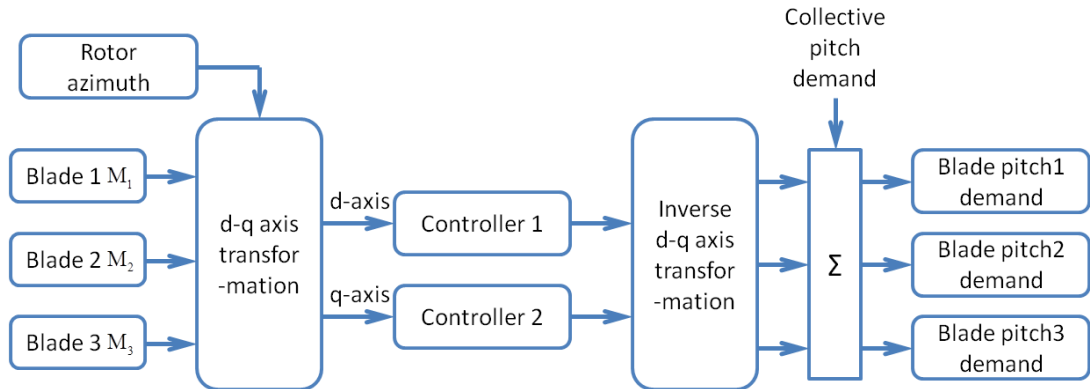


Figure 2.2: Individual pitch control loop using d-q axis transformation

Individual Blade Control

Modifications on the central controller are often necessary to accommodate the IPC, which make the technology difficult to be applied on existing turbines. The development of sensor technology improves IPC but it still faces problems such as being model dependent and not completely separated from the central controller. To address these problems, a novel approach ‘the Individual Blade Control’ (IBC) is proposed to reduce the unbalanced rotor loads [24, 25].

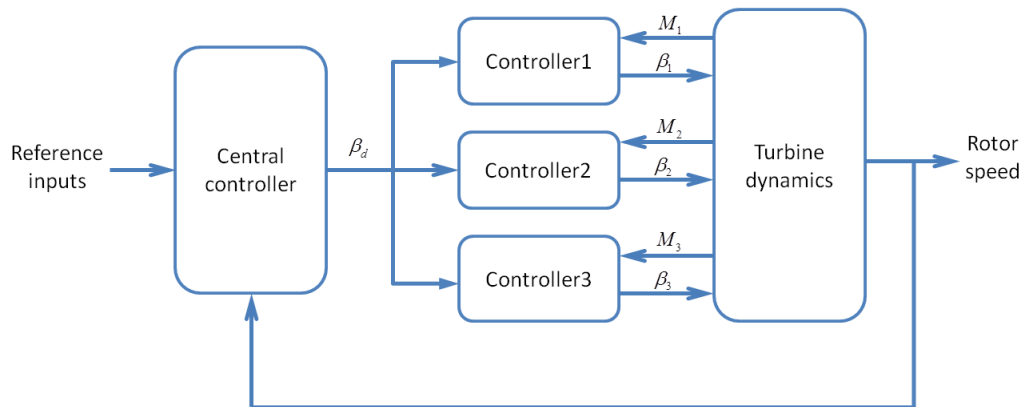


Figure 2.3: The structure of the IBC [26]

IBC achieves load reduction locally at each blade and can be separated from the central controller. The structure of the IBC is illustrated in Figure 2.3. M_1, M_2, M_3 are

measured blade loads and $\beta_1, \beta_2, \beta_3$ are pitch angle demands. The controller design for load reduction ideally only depends on the dynamics of a single blade, which is much simpler than the full wind turbine.

IBC has been applied to 2MW and 5MW wind turbine models. The effect of the IBC becomes much more significant as the size of the turbine increases. More than 20% life time fatigue load is reduced for the blades and near 50% on the rotor is observed for the 5MW turbine. Compared to IPC, IBC shows some obvious advantages, e.g. there is no need to communicate with the central controller in the nacelle.

2.3 Supergen 5MW Wind Turbine Model

The calculations and simulations in this thesis are based on the Supergen 5MW exemplar wind turbine. All the parameters of the wind turbine are listed in Appendix A.

2.3.1 Wind Turbine Modelling

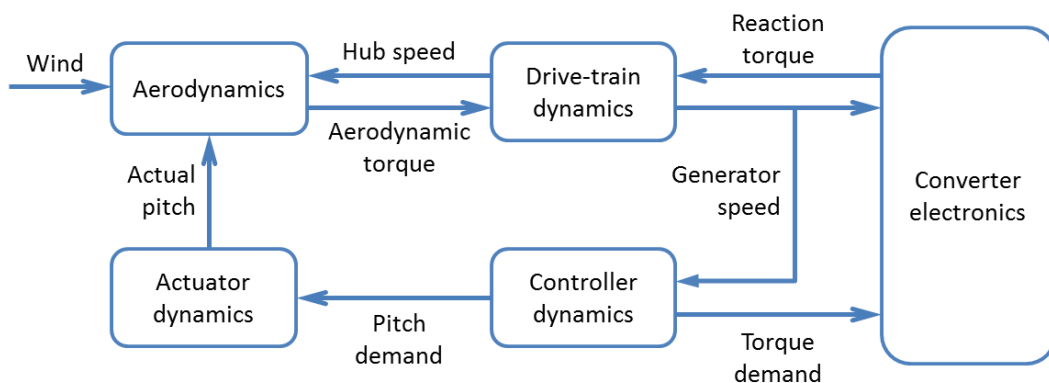


Figure 2.4: Dynamic model of the wind turbine

As shown in Figure 2.4, the 5MW wind turbine dynamic model includes wind speed, aerodynamics, drive-train dynamics, actuator dynamics, converter electronics and control dynamics. The derivation of these dynamics used here in the Simulink

Chapter 2. Overview of Wind Turbine and Controller

simulation for the controller design is described in detail in [27] and [28]. (See Figure C.2 to C.4 in Appendix C)

Aerodynamics

The aerodynamic torque T_f , is calculated from the Blade Element Momentum (BEM) theory, which is a combination of two methods using different approaches. One method is the momentum theory, which treats the rotor as a solid disc during the operation of a wind turbine. When air particles travel through the rotor disc, a change in static pressure occurs across the rotor disc, causing the air particles to slow down, thus losing momentum. Power extracted from the air by the rotor disc can hence be calculated. The other one is blade element theory, which involves dividing up the blade into a sufficient number of elements and calculating the flow at each one. The overall performance characteristics are determined by numerical integration along the blade span.

The aerodynamic torque depends nonlinearly on the wind speed U , the rotor speed Ω and the pitch angle of the rotor blades β , such that

$$T_f = \frac{1}{2} \rho \pi U^2 R^3 \frac{C_p(\lambda, \beta)}{\lambda} \quad (2)$$

where ρ is the air density, R is the rotor radius, C_p is the power coefficient and λ is the tip-speed ratio which is defined by the ratio between the speed of the tip of the blade and the wind speed. C_p is a nonlinear function of λ and β . The tip speed of the blade is calculated using the rotational speed of the rotor and its radius.

$$\lambda = \frac{R\Omega}{U} \quad (3)$$

Effective Wind Speed

In [18], a concept of effective wind speed is proposed, which is an average wind speed over the rotor. The authors develop an explicit solution for the effective wind speed. It is a filtered point wind at the hub and is uniform over the rotor area. The effective

Chapter 2. Overview of Wind Turbine and Controller

wind speed, for a single torque or moment can be expressed in the form of a transfer function:

$$v_{effective} = \frac{\frac{1}{\sigma} \cdot \left(s + \frac{\sqrt{2}}{\sigma}\right)}{\left(s + \frac{\sqrt{2}}{\sqrt{a'}\sigma}\right) \cdot \left(s + \frac{\sqrt{a'}}{\sigma}\right)} \cdot v_{pw} \quad (4)$$

where v_{pw} is the point wind speed, σ and a' are defined as follows

$$\sigma = \frac{\gamma R}{\hat{v}} \quad (5)$$

where γ is the turbulent wind speed decay factor, suggested values are $\gamma = 1.3$ and $a' = 0.55$, R is the rotor radius and \hat{v} is the point wind speed averaged over time by a 1st order filter of the form:

$$\hat{v} = \frac{k_2}{s + b} \cdot v_{pw} \quad (6)$$

The point wind speed v_{pw} can either be calculated from the transfer function with the Dryden spectrum or be taken from an external source such as Bladed.

The basic format of the Dryden spectrum with frequency in rad/s is:

$$S_D(\omega) = \frac{1}{2\pi} \frac{k_1^2}{(\omega^2 + a^2)} \quad (7)$$

The two parameters a and k_1 are selected to be the best fit approximation to the Von Karman spectrum as suggested in [18]:

$$a = 1.14(\bar{U}/l_u); k_1 = \sigma_v \sqrt{2a} \quad (8)$$

The advantage of using Dryden filter is that the wind speed fluctuation can be easily modelled by the following transfer function

$$v_{pw}(s) = \frac{k_1}{s + a} \cdot w(s) \quad (9)$$

where $w(s)$ is the white Gaussian noise.

In this study, the effective wind speed $v_{effective}$ is used in equation (1) to calculate the aerodynamic torque.

Drive-train Dynamics

It can be seen from Figure 2.5, the dynamics of the drive-train can be represented by the linear lumped parameter model [16]. The losses in the drive-train are represented as viscous damping on the low-speed and high-speed shafts. Most of the damping is external damping, e.g. losses in the gearbox, which is related to the absolute rotation of the drive-train. Internal damping, e.g. internal losses from shafts twisting, is related to the relative rotation of parts of the drive-train.

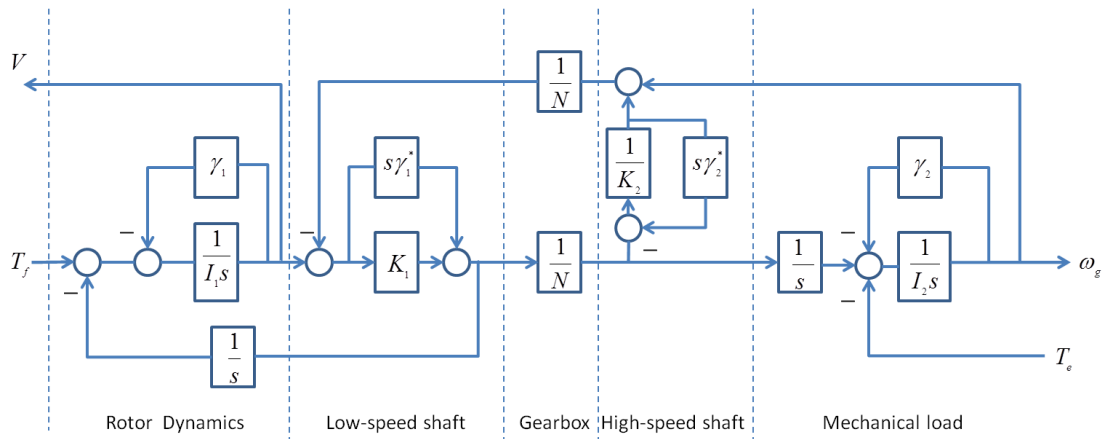


Figure 2.5: Drive-train model [16]

I_1 and I_2 represent the inertia of the rotor and generator. γ_1 and γ_2 are external damping coefficient of low-speed shaft and high-speed shaft. N is the gearbox ratio. K_1 and K_2 represent the stiffness of the low-shaft and high-shaft respectively. γ_1^* and γ_2^* are internal damping coefficient of low-speed shaft and high-speed shaft.

2.3.2 Supergen Baseline Controller

The operating strategy is illustrated in Figure 2.6. Depending on the operational behaviour of the wind turbine varying with the wind speed, four modes in the whole operation range are distinguished [29].

Mode 1 is the first constant speed section, when the generator torque is adjusted dynamically to regulate the generator speed at constant setting ω_0 . When the wind speed further increases, the generator speed is increased to maximize the energy capture. This stage is called mode 2. During this time, the generator speed is regulated by controller to follow $C_{p_{max}}$ curve. Mode 3 starts when the generator torque reaches the rated value T_1 . This is the second constant speed section. The generator speed is kept constant at ω_1 in this mode. Once the generator torque T_{set} is reached, the wind turbine enters into above rated operation, where the generator speed is controlled by pitch controller.

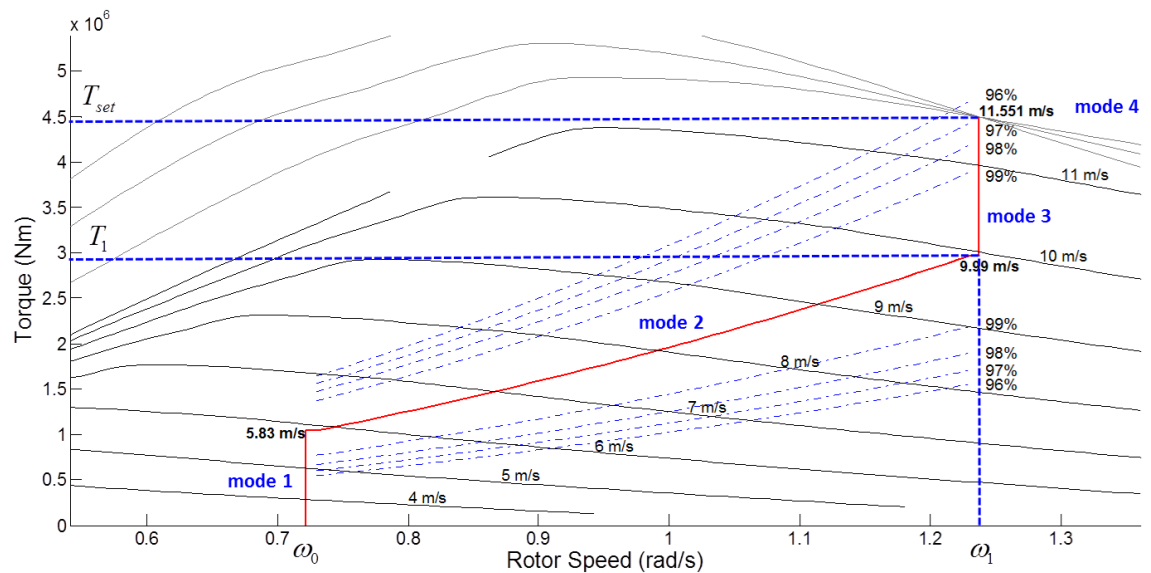


Figure 2.6: Ideal operating strategy of the Supergen 5MW wind turbine

Chapter 2. Overview of Wind Turbine and Controller

The Supergen baseline controller contains a below rated controller and an above rated controller as well. In below rated wind speed, the controller aims to reject low frequency disturbances whilst providing a bandwidth of at least 1 rad/s and to have good high frequency roll off. In above rated wind speed, the controller employs gain-scheduling techniques, which allow the controller to be used for the full operational range. Due to the complexity of the wind field, it is impossible to give exact gain and phase margins, however practical experience suggests a 10dB gain margin and a 60 degree phase margin. As wind turbines increase in size, gain margin and phase margin become narrower, great care must be taken when designing the above rated controller. Much like the below rated controller, it is necessary to obtain a bandwidth of at least 1 rad/s, reject low frequency disturbances and have good high frequency roll off.

Chapter 3

LIDAR Techniques

3.1 Overview of LIDAR Techniques

Types of remote wind measurements

A number of new technologies for measurement of fluid velocity have been developed in recent years [30]. A brief review of the characteristics of these technologies is given in this section.

Laser Doppler Anemometry (LDA) or Laser Doppler Velocimetry (LDV) is the technique of using Doppler shift in a laser beam. LDA provides a target measuring (focusing) distance of 150 m. The maximum length of the focal region is 40 m. Its measure distance is short and the applications are quite limited.

Particle Imaging Velocimetry (PIV) is to take snapshots of particles with a digital camera. With the images, it is possible to determine the speed and related properties of fluids. Nevertheless, in atmospheric conditions, it is necessary to add small particles to fluids previously, so it is not suitable for wind speed measurement. Doppler Global Velocimetry (DGV) is able to determine speeds of fluids by detecting frequencies of backscattered signals according to the Doppler effect, but this technique is not appropriate for wind industry due to its complexity.

Chapter 3. LIDAR Techniques

LIDAR and SODAR (SOund Detection And Ranging, or ‘acoustic radar’) are the two remote sensing techniques used today in wind energy application. Both techniques employ the Doppler effect to detect the movement of air in the Atmospheric Boundary Layer (ABL) and infer wind speed and direction [31].

SODAR is a ground-based remote sensing instrument that transmits (via speakers) a short acoustic sinusoidal pulse (typically 50 ms) into the ABL, and then listens for return signals for a short period of time. It measures the sound waves that are scattered back by turbulence caused by the thermodynamic structure of the atmosphere. Both the intensity and the Doppler shift of the returns can be used to determine wind speed and direction and the turbulent structure of the lower atmosphere. SODARs consisting of 3 or more beams at different angles to the vertical allow a three-dimensional vertical wind profile to be obtained.

SODAR has been applied in the wind industry successfully in the past few years. However, it is easily disturbed by noise from the turbine, and the emitted sound beam will be interfered by the blades, the ground, and so on, all this makes it impossible to get the accurate measurement.

Owing to development of fibre-optic telecommunication, it is possible to transmit information from one place to another by sending pulses of light through an optical fibre. LIDAR can be used for measuring wind profiles, distributions, directions, shears and veers. Its accuracy is well proven from independent studies, and its cost has been reduced in recent years. This has led to increased popularity of this technology in the wind industry.

Basic principle of coherent LIDAR [32]

LIDAR involves the emission of a coherent light beam and detection of the weak return reflected or scattered from a distant target. The technique provides a means to measure the line-of-sight component of wind speed via detection of the Doppler shift for light backscattered from natural aerosols in the atmosphere.

The principle by which coherent laser radar measures the velocity of a target is deceptively simple: a beam of coherent radiation illuminates the target, and a small fraction of the light is backscattered into a receiver. Motion of the target along the beam direction leads to a change $\delta\nu$ in the light's frequency via the Doppler shift, given by:

$$|\delta\nu| = \frac{2V_{LOS}}{c} \nu' = \frac{2V_{LOS}}{\lambda'} \quad (10)$$

where c is the speed of light (3×10^8 m/s), V_{LOS} is the component of target speed along the line of sight (i.e., the beam direction), ν' and λ' are respectively the laser frequency and wavelength. This frequency shift is accurately measured by mixing the return signal with a portion of the original beam and picking up the beats on a photo detector at the difference frequency. The essential features are shown in Figure 3.1.

There are mainly two kinds of LIDAR: Continuous Wave (CW) LIDAR and Pulsed LIDAR. The CW LIDAR emits a continuous unmodulated radiation beam. The detector output is then processed in discrete chunks at a rate determined by the signal processing and other system requirements.

Pulsed LIDAR, as its name implies, emits regularly spaced emissions of highly collimated light energy for a specified period of time (pulse length). Precision timing circuits then isolate the returned signals to a period of time that corresponds to a specified segment of radial distance along the beam called range gate. The

Chapter 3. LIDAR Techniques

backscattered signals contained within each gate are then processed to derive the radial velocities along the path of the LIDAR beam.

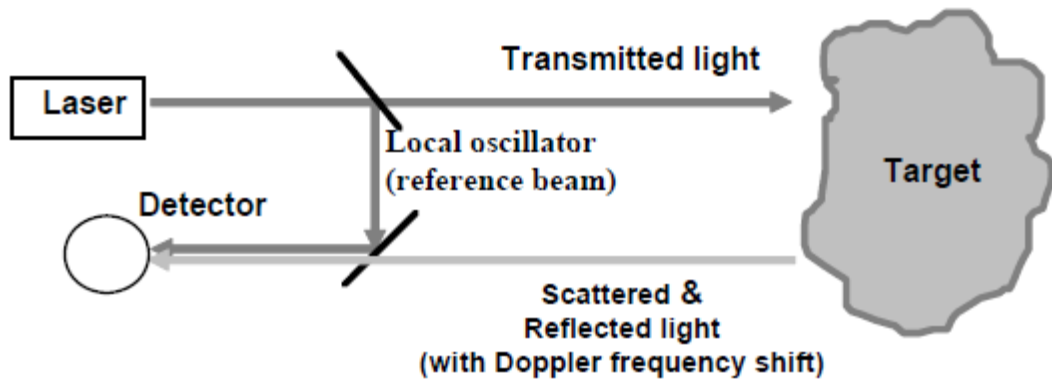


Figure 3.1: Generic bistatic LIDAR system [33]

Recently new LIDAR technologies have emerged which are targeted towards wind measurements over height ranges relevant to wind turbine applications, and which do not require the expense and logistics of liquid nitrogen cooling systems or stabilised optical platforms, usually needed for optical measurements. Many companies develop laser based wind profiler devices for wind measurements. SgurrEnergy in Scotland, ZephIR Lidar in England, LEOSPHERE in France and Renewable NRG Systems based in the United States are leading manufacturers.

Some LIDAR devices are already successfully used for wind speed and direction measurement, wind resource assessment, and wind turbine control system. ZephIR DM is developed by ZephIR Ltd. It gives wind measurement ranges from 10 metres to 300 metres. It measures both average wind speed and shear across the full rotor swept diameter, and specific hub height wind speed and direction. The speed range of ZephIR DM is 1m/s to 70m/s with speed accuracy variation of 0.1m/s. In addition, it can be operated across a specified temperature range of -40°C to +50°C [34].

3.2 LIDAR Measurement Theory

In this research, the coordinate system shown in Figure 3.2 is used for the analysis of LIDAR performance. -z is the direction of gravity and x is pointing in the downwind direction, θ is the measurement angle. The angle between the LIDAR beam and the wind speed vector is noted as ϕ . Therefore, the detected radial wind velocity is given by

$$v_{dec} = \sqrt{x^2 + y^2 + z^2} \cos(\phi) \quad (11)$$

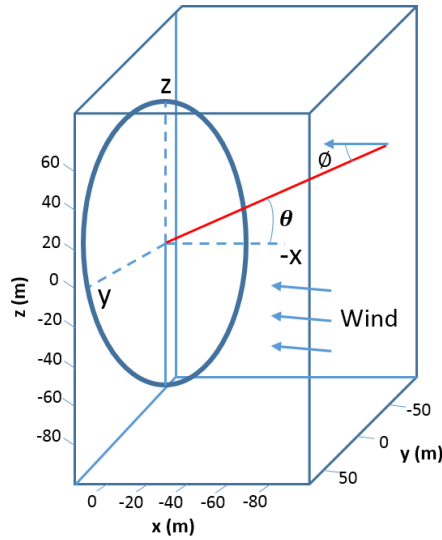


Figure 3.2 Coordinate system for LIDAR measurement [35]

LIDAR measured wind speed is the average value of wind speed at different points on the scan radius, as shown in Figure 3.3. Variables referred to in the analysis of a spinning LIDAR including preview distance d , and scan radius r . The angle between scan radius and x direction is ψ .

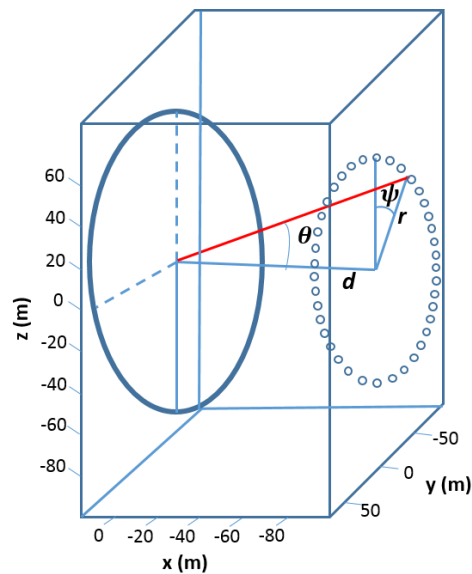


Figure 3.3 Coordinate system for LIDAR measurement with scan radius

3.3 LIDAR for Wind Turbine Control

A brief review of the implication of LIDAR in wind turbine control is presented in this section. Currently, feedforward control strategy and model predictive control are two main techniques of using LIDAR measurements.

Feedforward control using LIDAR

Three types of feedforward blade pitch controllers are investigated and evaluated in [36] and [37]. They are non-causal series expansion, preview control, and optimized finite impulse response (FIR) filter. All three feedforward controllers are augmented to a baseline controller.

The non-causal series expansion controller is simulated in both individual pitch and collective pitch form. In the individual pitch condition, there are three copies of the feedforward controller, everyone is fed with wind speed measurement and controls a blade. This individual pitch feedforward control is then added on to the individual

Chapter 3. LIDAR Techniques

pitch baseline feedback controller. It is shown from the simulation studies that the individual pitch and the collective pitch version have similar results. Non-causal series expansion reduces blade root bending loads, but causes unacceptable increases in tower sway at the same time.

Preview control includes a preview of the wind speed disturbance and a cost function. The control is designed to be added to a collective pitch PI controller. Preview control is able to reduce both blade and tower loads on the linear model as well as in simple uniform wind field simulations. However, when simulated in turbulent wind conditions, like the non-causal series expansion control, preview control increases tower sway.

A brand new FIR filter is proposed as the third feedforward controller. It uses a genetic algorithm to simulate thousands of random possible FIR filters. Among the three types of feedforward controller, the performance of optimized FIR filter is the best. It reduces loads on different parts of the turbine by varying amounts, while maintaining rated power and rotor speed without significantly increasing pitch rate.

In [38], the baseline controller is extended with a LIDAR-assisted feedforward controller. The pitch rate increment is calculated. The results illustrates that when the turbine is loaded with an 'extreme operating gust', compared with baseline controller, the feedforward controller reduces the peak deviation of rotor speed and the maximum tower base fore-aft moment. In terms of fatigue loads, feedforward controller lessens the impact of the wind disturbance on the rotor speed and on the tower base fore-aft bending moment below the 1P frequency. The lifetime Damage Equivalent Loads (DEL) for the tower base fore-aft moment is decreased compared with the baseline controller.

Chapter 3. LIDAR Techniques

Na Wang et al design two feedforward controllers for wind turbine rotor speed regulation and component load reduction when the turbine is operating in above rated wind speed. The first one is an adaptive controller based on a filtered-x recursive least square (FX-RLS) algorithm. The second one is a nonadaptive controller based on a zero-phase-error tracking control (ZPETC) technique. Both controllers are combined with a collective pitch proportional-integral (PI) feedback controller. ZPETC feedforward controller reduces the blade loads but increases the tower loads, while the FX-RLS feedforward algorithm improves the performance in both tower and blade bending moment mitigation [39].

Literature review suggests that feedforward control is an effective approach to utilize LIDAR technique. Applying LIDAR measurements in above rated pitch control can be beneficial.

Model predictive control using LIDAR

Model predictive control (MPC) has proved to be an effective tool to be applied in multivariable constrained systems, such as wind turbines. Many LIDAR-assisted MPC design approaches have been proposed in the literature.

In [40], an approach is proposed to deal with optimization problem of MPC. The nonlinear wind turbine model is linearised at different operating points, which are determined by the effective wind speed on the rotor disc. LIDAR wind speed measurement is used as a scheduling parameter. This method is robust with respect to the error in LIDAR measurement. The nonlinear model predictive control algorithm using future wind speeds in the prediction horizon is presented by L. C Henriksen et al. The method is applied in both partial and full load operation. For complex wind structures, e.g. turbulence, information of future wind speeds would be able to help the wind turbine to produce more power at partial load operation. For full load operation, the generator speed is better controlled when the information of future

Chapter 3. LIDAR Techniques

wind speed is included in the prediction horizon [41]. In [42], the performance of the nonlinear model predictive controller using LIDAR is compared with the feedback controller. Simulation results indicate that tower and blade load reductions without degradation in power production can be gained with the nonlinear model predictive control.

Besides feedforward control and MPC, there are some other control strategies that have potential to use LIDAR measurement, e.g. Disturbance Accommodating Controller (DAC).

In [32], the shear disturbance is measured instead of estimated, which increase the accuracy of DAC controller. Normal DAC and DAC using LIDAR give similar blade flap-bending moment response for the low shear case, while the DAC using LIDAR reduces the blade flap-bending moment response in the high shear case.

Chapter 4

Design of Feedforward Controller

According to the discussion in Chapter 3, LIDAR is able to provide preview information of wind disturbances at various distances in front of wind turbines. This feature can be used in feedforward control to improve the technique of disturbance rejection. This research augments the feedback pitch controller with a feedforward control term to alleviate turbine loads in above rated wind speed conditions. The feedforward controller is designed based on Supergen 5MW wind turbine model, which has been introduced in section 2.3.2.

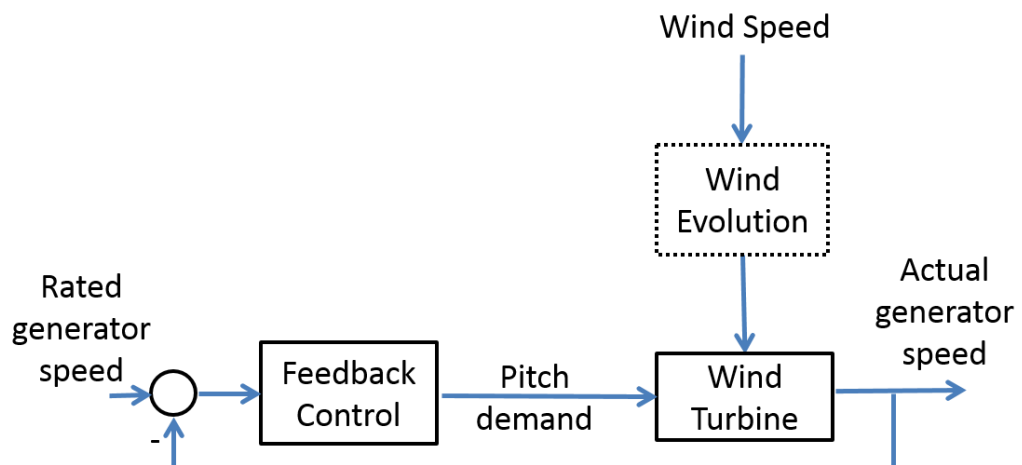


Figure 4.1: Block diagram of feedback baseline control [43]

The conventional wind turbine feedback control diagram is shown in Figure 4.1. The evolution model block in the figure reflects the process from wind resource to the

Chapter 4. Design of Feedforward Control

wind finally approaches on the blades of the wind turbine. The turbine wind speed and the pitch command from feedback controller are shown as the input of the wind turbine. The aim of the feedback control system is to minimize the difference between actual generator speed and rated generator speed.

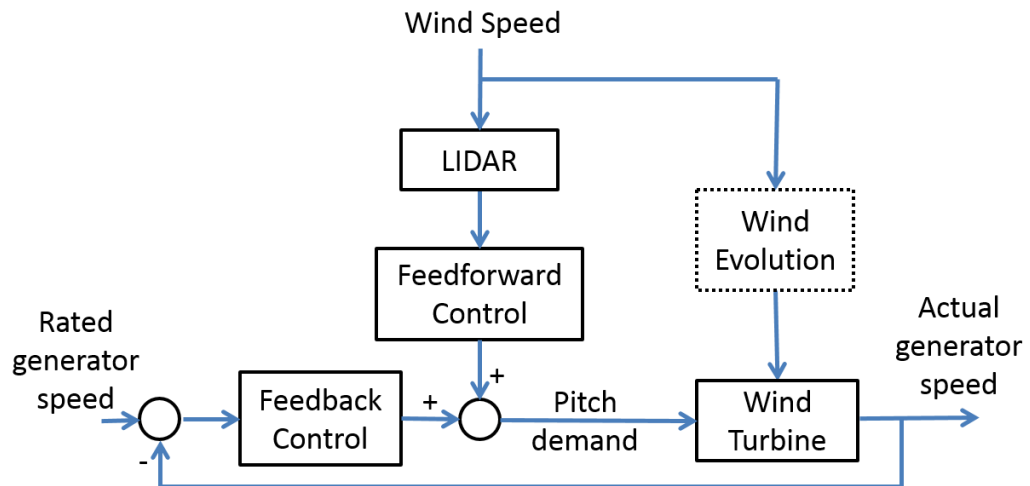


Figure 4.2: Combined feedback and feedforward control

Figure 4.2 shows a model-inverse-based strategy for designing feedforward controllers. The feedforward controller is used to cancel the effect from the turbulence in wind speed on the wind turbine generator speed. In Figure 4.2, the total pitch demand is the combination of the pitch demand from feedback controller and the output of feedforward controller.

4.1 The LIDAR Preview

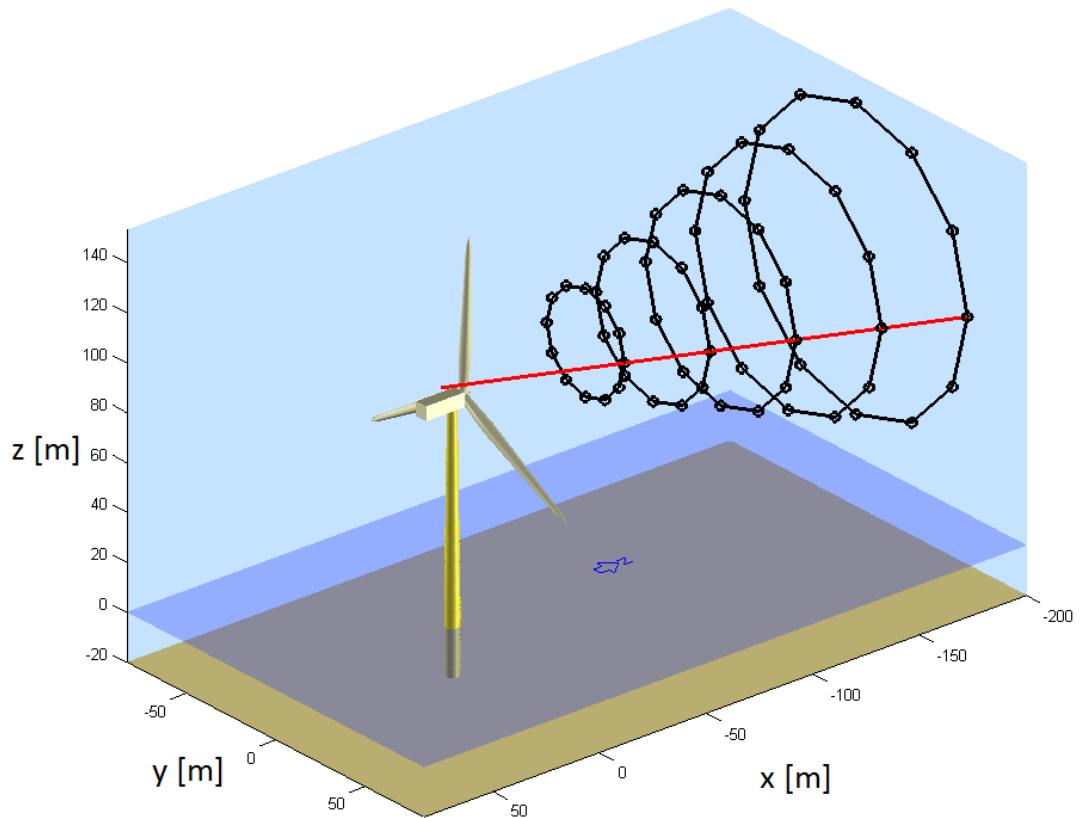


Figure 4.3: Scope of simulated LIDAR measurements [11]

According to the feedforward control loop in Figure 4.2, LIDAR measured wind speed is fed into the feedforward controller. In this research, the controller design uses simulated LIDAR measurements instead of real LIDAR signal. The strategy of simulating LIDAR measurements is depicted in Figure 4.3. Taylor's frozen turbulence hypothesis is employed, which assumes the turbulent wind field to be unaffected when approaching the rotor and moving with average wind speed [44]. Figure 4.3 shows the chosen circle scan, which provides 12 measurements in 5 focus distances equally distributed between 42.7m and 85.3m. Only the component of the wind

vector in laser beam direction (line of sight wind speed) is detected. It is constructed by averaging over the circular trajectory.

4.2 The Feedforward Controller

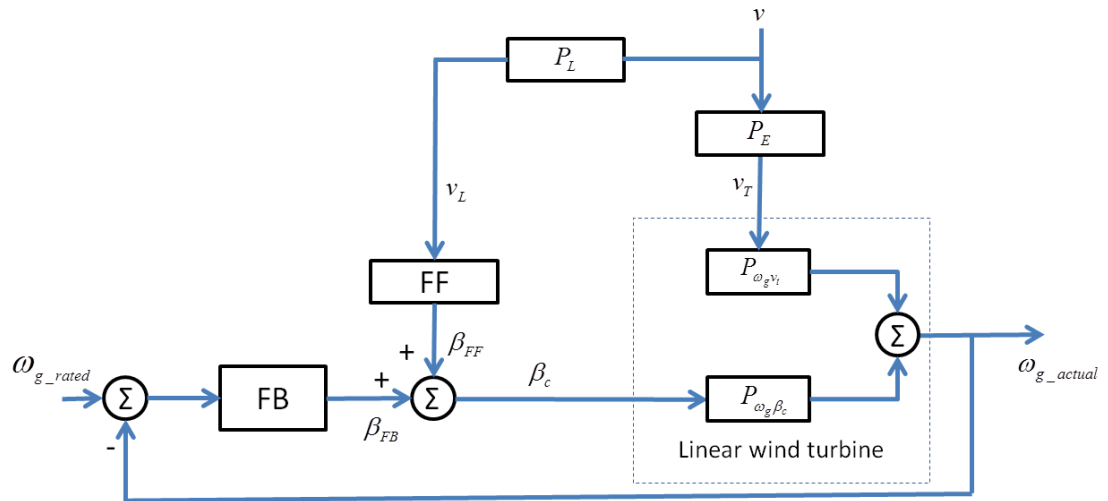


Figure 4.4: Feedforward control scheme

The feedforward control scheme in Figure 4.4 is developed from the block diagram of feedback/feedforward control loop in Figure 4.2. v denotes wind field, and v_T is the turbine wind speed, which indicates the wind speed approaches the turbine blades. v evolves to v_T on its way to the turbine and disturbs the wind turbine system. System P_E represents this evolution. The measurement of the wind field in front of the turbine by a LIDAR system is v_L (line of sight wind speed). P_L is the LIDAR system transferring v to v_L . FB is the feedback controller and FF is the feedforward controller. The linear wind turbine model includes transfer functions $P_{\omega_e \beta_c}$ and $P_{\omega_e v_t}$. $P_{\omega_e \beta_c}$ maps collective blade pitch error β to generator speed error ω_e and $P_{\omega_e v_t}$ maps deviation from nominal wind speed v to generator speed error ω_e .

Chapter 4. Design of Feedforward Control

The output of feedforward controller β_{FF} is added to the pitch angle β_{FB} of collective pitch feedback controller. The primary control goal of the whole control system is to maintain the actual greater speed ω_{g_actual} at rated generator speed value ω_{g_rated} in the presence of varying wind v above the rated wind speed by adjusting the total pitch angle command β_c . P_{LT} is the relationship between v_T and v_L , see Figure 4.5.

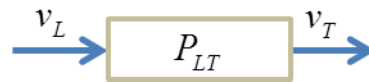


Figure 4.5: The Relationship between v_L and v_T

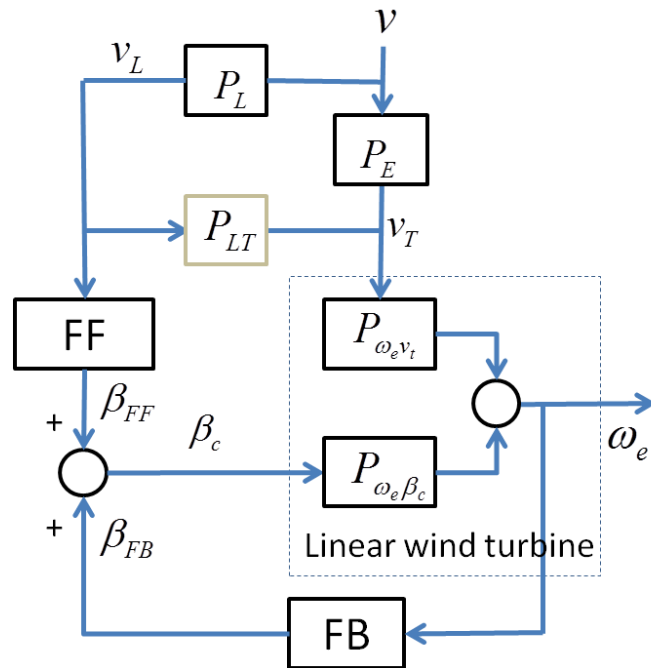


Figure 4.6: Modified feedforward control scheme

Based on Figure 4.4, a modified feedforward control scheme is developed and shown in Figure 4.6, where ω_e is the generator speed error ($\omega_{g_rated} - \omega_{g_actual}$). The desired generator speed error is zero [45]. It can be seen from Figure 4.6 that $v \cdot P_L = v_L$ and $v \cdot P_E = v_T$, therefore, $P_{LT} = P_E \cdot P_L^{-1}$.

Chapter 4. Design of Feedforward Control

According to the control loop in Figure 4.6, we have

$$(v \cdot P_L \cdot FF + \omega_e \cdot FB) \cdot P_{\omega_e \beta_c} + v \cdot P_E \cdot P_{\omega_e v_t} = \omega_e \quad (12)$$

Since $\omega_e = 0$,

$$v \cdot P_L \cdot P_{\omega_e \beta_c} \cdot FF + v \cdot P_E \cdot P_{\omega_e v_t} = 0 \quad (13)$$

The feedforward controller is solved as

$$FF = -P_{\omega_e \beta_c}^{-1} \cdot P_{\omega_e v_t} \cdot P_E \cdot P_L^{-1} \quad (14)$$

where $P_{\omega_e \beta_c}^{-1}$ and $P_{\omega_e v_t}$ can be obtained from turbine modelling, but wind evolution P_E and LIDAR system P_L are very complex and difficult to model. In this study, the part $P_E \cdot P_L^{-1}$ is approximated by a transfer function

$$P_{LT} = P_E \cdot P_L^{-1} = \frac{S_{LT}}{S_{LL}} \quad (15)$$

where S_{LT} is the cross spectrum between the LIDAR measurements and the turbine wind speed, S_{LL} is the auto spectrum of the LIDAR measurements.

Finally, the feedforward controller is represented as

$$FF = -P_{\omega_e \beta_c}^{-1} \cdot P_{\omega_e v_t} \cdot P_{LT} \quad (16)$$

4.2.1 Cross Correlation Study

In order to calculate S_{LT} and S_{LL} , some theories related to cross correlation and cross spectrum are explained in this subsection.

Let $v(t, x)$ be the wind speed fluctuation at time t and position x . The cross correlation between $v(t, d)$, the current wind speed fluctuation at displacement d and $v(t + \delta t, 0)$, the wind speed fluctuation δt seconds later at displacement 0, is

$$R_{v(t',d)v(t'+\delta t,0)}(t + s, t + \delta t) = E[v(t + s, d)v(t + \delta t, 0)] \quad (17)$$

Assuming stationary,

$$R_{v(t,d)v(t',0)}(t + s, t + \delta t) = R_{v(t,d)v(t',0)}(s - \delta t) \quad (18)$$

Hence, $S_{v(t,d)v(t'+\delta t,0)}(\omega)$, the cross spectrum of $v(t, d)$ and $v(t + \delta t, 0)$, is

$$\begin{aligned} S_{v(t,d)v(t'+\delta t,0)}(\omega) &= F\{R_{v(t,d)v(t',0)}(s - \delta t)\} \\ &= e^{-i\omega\delta t} F\{R_{v(t,d)v(t',0)}(s)\} \\ &= e^{-i\omega\delta t} S_{v(t,d)v(t',0)}(\omega) \end{aligned} \quad (19)$$

where $F\{\cdot\}$ is the Fourier transform, $S_{v(t,d)v(t',0)}(\omega)$ is the cross spectrum of $v(t, d)$ and $v(t, 0)$. Therefore, the cross spectrum, between the mean wind speed fluctuations with the averaging areas displaced by d and time by δt , can be expressed as the cross spectrum, between the mean wind speed fluctuations with the averaging areas displaced by d with no time displacement, scaled by $e^{-i\omega\delta t}$.

4.2.2 Wind Speed Simulation

Bladed uses a 3-dimensional turbulent wind field with defined spectral and spatial covariance characteristics to represent real atmospheric turbulence. This option will give the most realistic predictions of loads and performance in normal conditions.

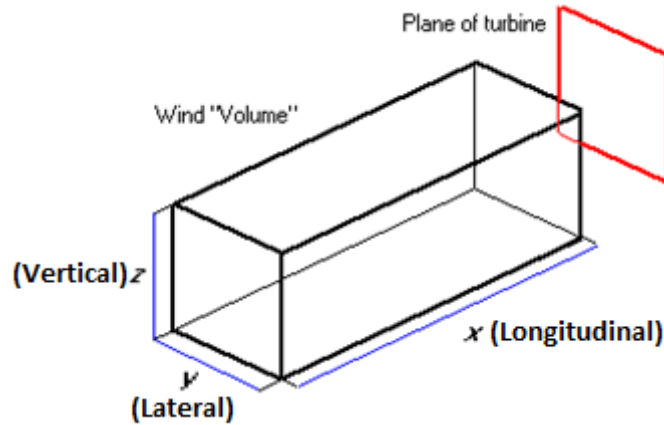


Figure 4.7: 3D wind volume simulated by Bladed

In Bladed, wind speed is displayed as a vector of 3 components: Longitudinal component $x(t)$, Lateral component $y(t)$ and Vertical component $z(t)$, see Figure 4.7. The parameters set up for the wind field simulation are listed in Table 4.1 to 4.3.

Chapter 4. Design of Feedforward Control

Table 4.1: Parameters of the turbine

Number of blades	3
Nominal rotor diameter	80m
Tower height	60m
Total hub height	61.5m

Table 4.2: Characterises of turbulence

Spectrum Type		Von Karman(improved)
Number of components		3
Width of field	m	100
Number of points across		15
Height of field	m	105
Number of points in height		15
Length of field	m	1804.8
Alongwind spacing	m	0.88125
Turbulence seeds		1
Mean wind speed	m/s	12
Height above ground	m	61.5
Roughness length	m	0.1
Latitude	deg	49.9999

Table 4.3: Characterises of 3D turbulence

Turbulence length scales		Component of turbulence		
		Longitudinal	Lateral	Vertical
Along X (Longitudinal)	m	244.671	58.8681	21.1883
Along Y (Lateral)	m	79.6605	76.6657	13.7971

Chapter 4. Design of Feedforward Control

Along Z (Vertical)	m	59.2508	28.5117	20.5243
Turbulence intensities:	%	16.0108	12.5465	8.92472

According to the LIDAR scan trajectories in Figure 4.3 and Bladed display of wind field in Figure 4.7, $v_T(t_T, x_T)$ and $v_{Li}(t_{Li}, x_{Li})(i = 1, \dots, 6)$ are points sampled from Bladed wind field in the x direction to represent the turbine wind speed and LIDAR measurements. $v_T(x_T = 0m)$ is assumed as the turbine wind speed, which is the mean wind fluctuation over the turbine plane. $v_{Li}(t_{Li}, x_{Li})(i = 1, \dots, 6)$ are assumed as LIDAR measurements with preview distances of 30m, 60m, 90m, 120m, 160m and 190m respectively ($x_{L1} = 30m, x_{L2} = 60m, x_{L3} = 90m, x_{L4} = 120m, x_{L5} = 160m, x_{L6} = 190m$). Each wind speed is the mean wind fluctuation over an area lying in the y-z plane. The distribution of all wind speed points is shown in Figure 4.8.

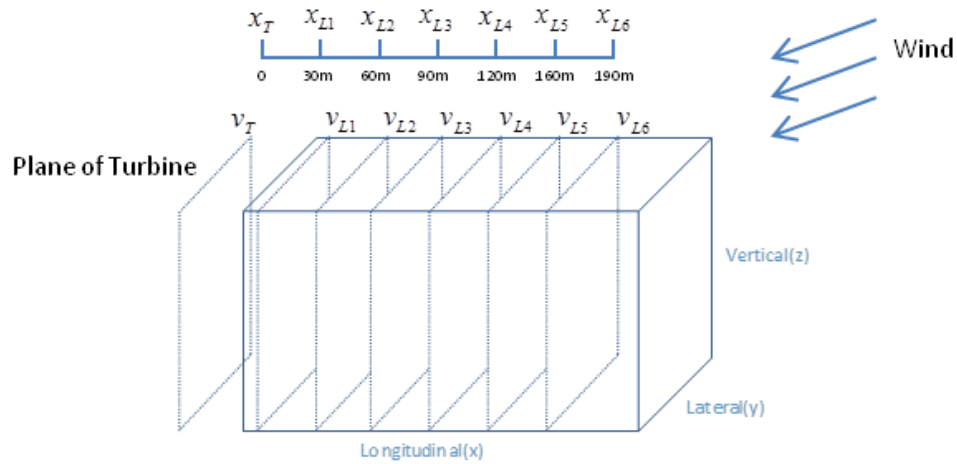


Figure 4.8: Distribution of $v_T(t_T, x_T)$ and $v_{Li}(t_{Li}, x_{Li})(i = 1, \dots, 6)$

In Figure 4.8, the wind speed evolves in the direction of distance x. There is no cross correlation between $v_T(t_T, x_T)$ and $v_{Li}(t_{Li}, x_{Li})(i = 1, \dots, 6)$. Therefore, the strategy of sampling points in the wind field is needed to be modified.

Chapter 4. Design of Feedforward Control

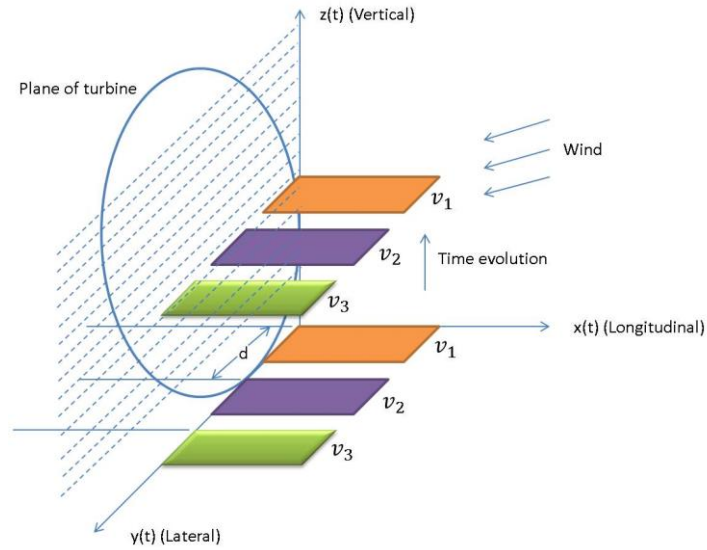


Figure 4.9: Schematics of wind speed sampling in Bladed

As the Bladed wind field is frozen and isotropic, the variation of the wind speed fluctuation in the x direction at a point can be equally represented by the component in the y direction as well as the component in the z direction. Hence, as depicted in Figure 4.9, the cross correlation between the mean wind speed fluctuations over two areas displaced by a distance d in the x direction can be estimated from the areas lying in x - y planes separated by a distance of d in the y direction and the fluctuations in the z direction. Time evolution can be represented by moving the plates through the wind field in the z direction.

Hence, the distribution of turbine wind speed and LIDAR measurements can be modified from Figure 4.8 to Figure 4.10. $v_T(t_T, x_T)$ and $v_{Li}(t_{Li}, x_{Li})(i = 1, \dots, 6)$ represent mean wind fluctuations in x - y plane, with time evolution in the z direction.

Chapter 4. Design of Feedforward Control

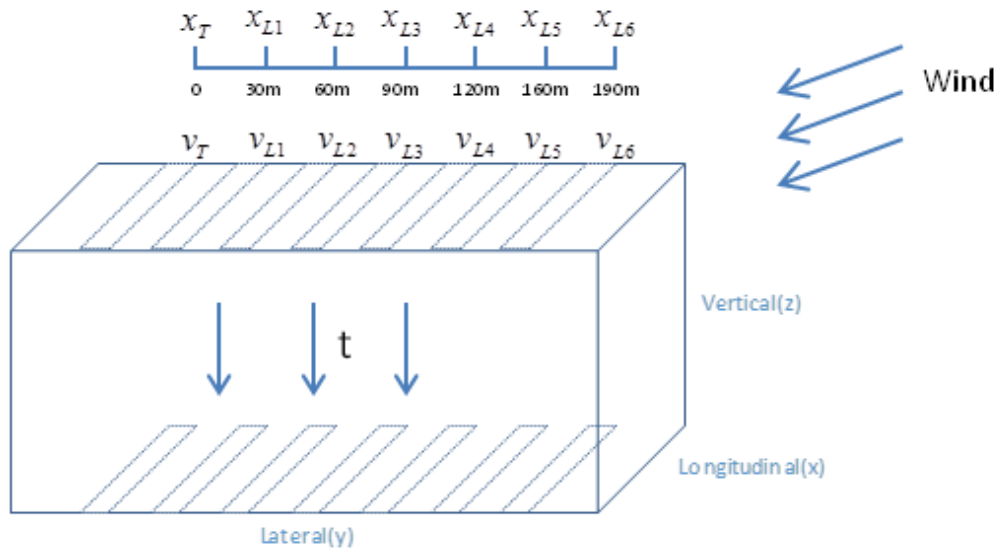


Figure 4.10: Modified distribution of the turbine wind speed and LIDAR measurements

Figure 4.11 shows lateral components of turbine wind speed v_T and LIDAR measurements v_{L1} , v_{L2} , v_{L3} . High similarity can be detected for the whole time range.

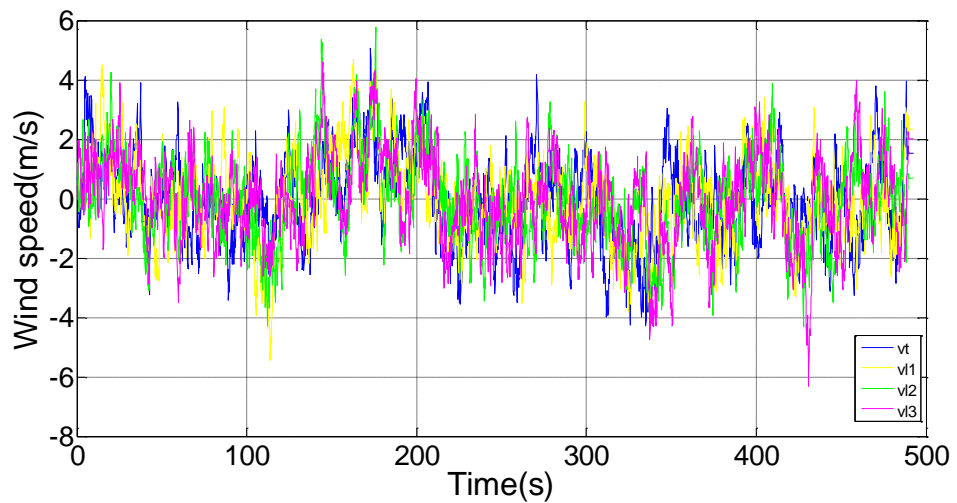


Figure 4.11: Lateral components of v_T , v_{L1} , v_{L2} and v_{L3}

4.2.3 Cross Correlation and Cross Spectrum

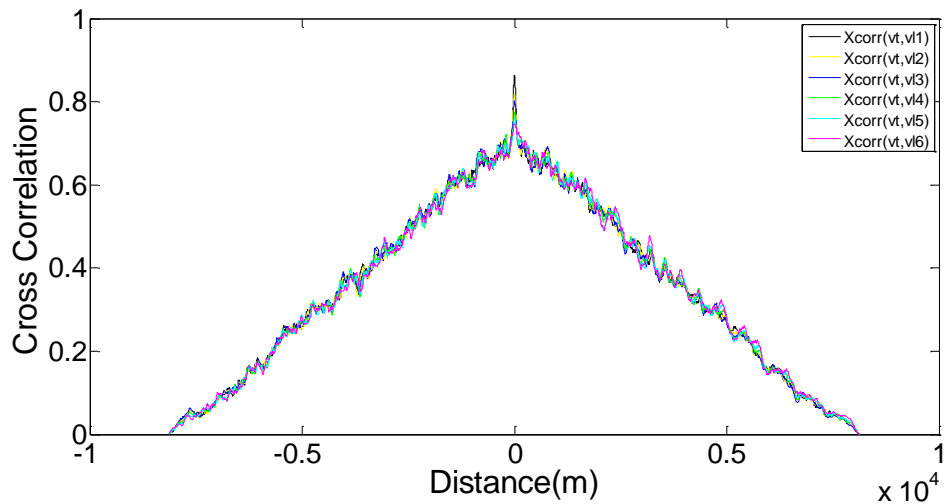


Figure 4.12: Cross correlation between the turbine wind speed v_T and LIDAR measurements

The results of the cross correlation between turbine wind speed and LIDAR measurements are depicted in Figure 4.12. A zoom-in figure is given below for distance range [-100m 100m].

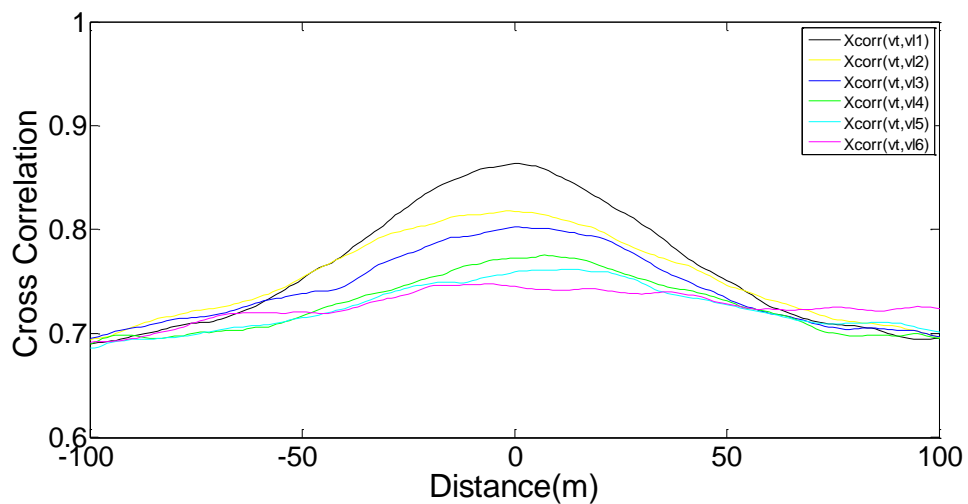


Figure 4.13: Zoom-in figure of cross correlation for distance axis between -100m to 100m

Chapter 4. Design of Feedforward Control

It can be seen from Figure 4.13 that the correlation coefficient varies with the preview distance. Within 50m, the coefficient decreases with the preview distance. The correlation of v_T and v_{L1} is larger than others. Outside 50m, the difference between correlations of v_T and $v_{Li}(t_{Li}, x_{Li})(i = 1, \dots, 6)$ is not obvious. Within 100m, all correlation coefficients are above 0.65. The correlation of v_T and v_{L1} has the largest maximum value 0.9. v_T and v_{L6} have the smallest maximum coefficient 0.73.

The cross spectrum of the turbine wind speed v_T and LIDAR measurements can be obtained from equation (17), see Figure 4.14. Figure 4.15 shows auto spectrum of $v_{Li}(t_{Li}, x_{Li})(i = 1, \dots, 6)$.

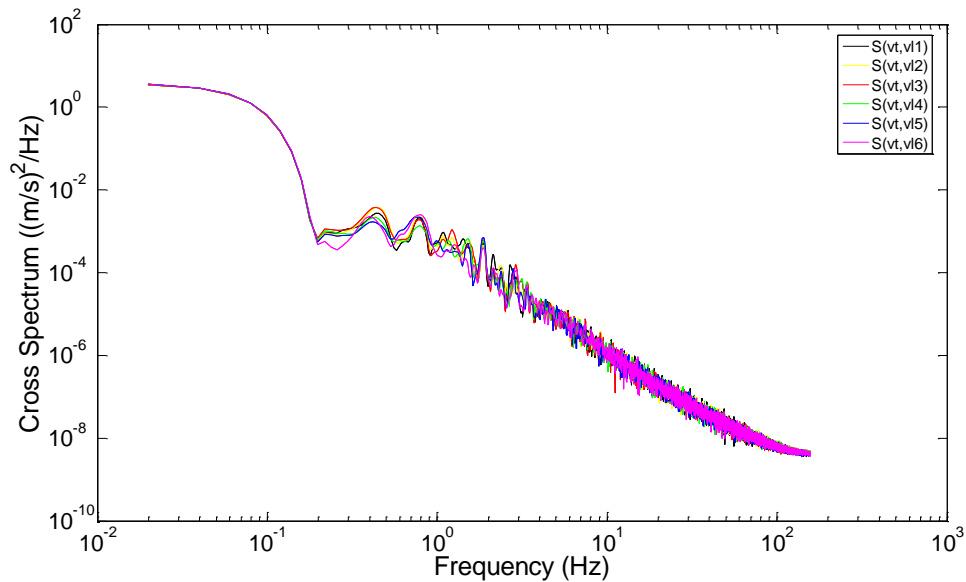


Figure 4.14: Cross spectrum of the turbine wind speed and LIDAR measurements

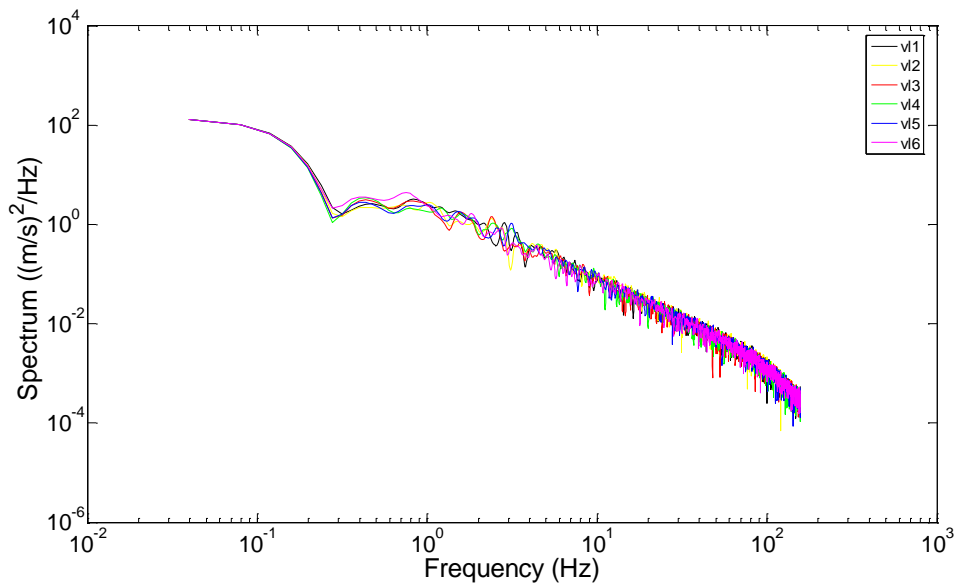


Figure 4.15: Auto spectrum of LIDAR measurements

Following the results of cross spectrum S_{LT} and auto spectrum S_{LL} , the transfer function P_{LT} in equation (14) is approximated by a first order low-pass filter:

$$P_{LT} \approx - \frac{8.102 \times 10^{-7}}{s + 0.02831} \quad (20)$$

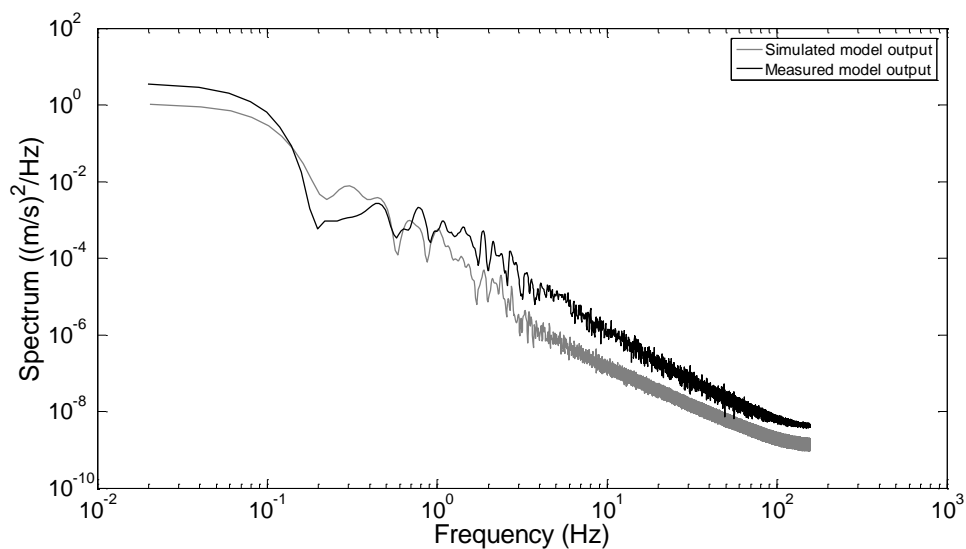


Figure 4.16: Comparison of simulated model output and measured model output

Chapter 4. Design of Feedforward Control

The transfer function model P_{LT} has been validated against cross spectrum $S(v_t, v_{t1})$, see Figure 4.16. It can be seen that the shapes of the simulated model output and the measured model output match well. Therefore, the transfer function is acceptable for the controller design.

4.2.4 Wind Turbine Model Linearisation

In this subsection, 5MW Supergen wind turbine model is linearised for feedforward controller design. The results of blade pitch angle, generator speed, turbine output power and tower fore-aft acceleration of feedback baseline control are compared with feedback/feedforward control.

It can be seen from equation (2) and (3) that the aerodynamic torque of a wind turbine T_f depends nonlinearly on three variables: wind speed U , blade pitch angle β and rotor speed Ω . In order to analyse the turbine with linear models, the nonlinear torque function is needed to be linearised following the Taylor series expansion theory. A Taylor series is a series expansion of a function about a point. Take an example, a two-dimensional Taylor series is an expansion of a real function $f(x, y)$ about a point (x_0, y_0) , which is given by

$$f(x, y) = f(x_0, y_0) + \left. \frac{\partial f}{\partial x} \right|_{x_0, y_0} (x - x_0) + \left. \frac{\partial f}{\partial y} \right|_{x_0, y_0} (y - y_0) \quad (21)$$

Aerodynamic torque of the wind turbine is then, locally to a specific operating point (β_0, ω_0, U_0) , expressed as:

$$\begin{aligned} T_f(\beta, \omega, U) = & T_f(\beta_0, \omega_0, U_0) + (\beta - \beta_0) \left. \frac{\partial T}{\partial \beta} \right|_{(\beta_0, \omega_0, U_0)} \\ & + (\omega - \omega_0) \left. \frac{\partial T}{\partial \Omega} \right|_{(\beta_0, \omega_0, U_0)} \\ & + (U - U_0) \left. \frac{\partial T}{\partial U} \right|_{(\beta_0, \omega_0, U_0)} \end{aligned} \quad (22)$$

Chapter 4. Design of Feedforward Control

Therefore, T_f is now linearised with respect to blade pitch angle β , generator speed ω and wind speed U , at any given equilibrium operating point, and with any small perturbation about their nominal values, it leads to:

$$\Delta T_f = K_\beta \Delta \beta + K_v \Delta \omega + K_u \Delta U \quad (23)$$

where

$$\begin{aligned} K_\beta &= \left. \frac{\partial T}{\partial \beta} \right|_{(\beta_0, \omega_0, U_0)} = \frac{1}{2} \rho \pi U_0^2 R^3 \left. \frac{\partial C_q}{\partial \beta} \right|_{(\beta_0, \omega_0, U_0)} = \frac{T_f(\beta_0, \omega_0, U_0)}{\beta_0} \left. \frac{\partial C_q / \partial \beta}{C_q / \beta} \right|_{(\beta_0, \omega_0, U_0)} \\ K_v &= \left. \frac{\partial T}{\partial \omega} \right|_{(\beta_0, \omega_0, U_0)} = \frac{1}{2} \rho \pi U_0 R^4 \left. \frac{\partial C_q}{\partial \lambda} \right|_{(\beta_0, \omega_0, U_0)} = \frac{T_f(\beta_0, \omega_0, U_0)}{\omega_0} \left. \frac{\partial C_q / \partial \lambda}{C_q / \lambda} \right|_{(\beta_0, \omega_0, U_0)} \\ K_u &= \left. \frac{\partial T}{\partial U} \right|_{(\beta_0, \omega_0, U_0)} = \frac{T_f(\beta_0, \omega_0, U_0)}{U_0} \left(2 - \left. \frac{\partial C_q / \partial \lambda}{C_q / \lambda} \right|_{(\beta_0, \omega_0, U_0)} \right) \end{aligned} \quad (24)$$

There are several ways to linearise the nonlinear wind turbine model: Software package Bladed, Sgurr ControlBox, or manual calculation using equations from (17) to (20). In this research, Bladed is used to obtain linear state-space model of the wind turbine. The state-space form is given in formulation

$$\begin{cases} \dot{x} = Ax + Bu \\ y = Cx + Du \end{cases} \quad (25)$$

In the simulation, 12 state variables are included in the state-space model: gearbox LSS angular displacement, gearbox LSS angular velocity, LSS angular displacement, LSS angular velocity, blade 0 actuator position state 2, blade 1 actuator position state 1, blade 1 actuator position state 2, blade 2 actuator position state 1, blade 2 actuator position state 2, blade 3 actuator position state 1 and two others. Details of the state-space models are given in Appendix B.1.

According to equation (14), $P_{\omega_e \beta_c}(s)$ and $P_{\omega_e v_t}(s)$ are needed to be obtained for the controller design. Both transfer functions can be converted from the state-space representation of the wind turbine system, see Appendix B.2.

In this research, the wind turbine model is linearised at two operating points. Point one is defined at pitch angle $\beta_0 = 0.15 \text{ deg}$, generator speed $\omega_0 = 120 \text{ rad/s}$ and

Chapter 4. Design of Feedforward Control

wind speed $U_0 = 12 \text{ m/s}$. Point two is defined at pitch angle $\beta_0 = 0.2113 \text{ deg}$, generator speed $\omega_0 = 120 \text{ rad/s}$ and wind speed $U_0 = 16 \text{ m/s}$. The model linearised at point one is model I and the model linearised at point two is model II. Two feedforward controllers are developed based on these two models.

Feedforward Controller for Model I:

The continuous transfer function $P_{\omega_e\beta_c}(s)$ from pitch angle error to generator speed error is discretized using zero-order hold discretization method, with sampling time 0.0125s, we get

$$P_{\omega_e\beta_c}(z) = \frac{B_1(z)}{W_1(z)} \quad (26)$$

in which

$$B_1(z) = -1.3052(z + 1.1518)z^{10} \quad (27)$$

$$\begin{aligned} W_1(z) = & (z^2 + 0.3156z + 0.624)(z^2 - 1.9796z + 0.9921) \\ & (z^2 - 1.9528z + 0.9562)(z^2 - 2.0022z \\ & + 1.0028) \\ & (z^2 - 1.9918z + 0.9923)(z - 1.0002)z \end{aligned} \quad (28)$$

The continuous transfer function $P_{\omega_e v_t}(s)$ from derivation from nominal wind speed to generator speed error is discretized in the same way as $P_{\omega_e\beta_c}(s)$ to

$$P_{\omega_e v_t}(z) = \frac{V_1(z)}{W_1(z)} \quad (29)$$

with

$$\begin{aligned} V_1(z) = & (2.6718 \times 10^{-5})(z^2 - 1.9952z + 1.0004) \\ & (z^2 - 1.9992z + 0.9997)(z^2 - 1.9992z + 0.9997) \\ & (z + 9.1775)(z + 1.0888)(z - 0.2666)(z \\ & + 0.1553)z \end{aligned} \quad (30)$$

$$W_1(z) = (z^2 + 0.3156z + 0.624)(z^2 - 1.9796z + 0.9921) \quad (31)$$

Chapter 4. Design of Feedforward Control

$$\frac{(z^2 - 1.9528z + 0.9562)(z^2 - 2.0022z + 1.0028)}{(z^2 - 1.9918z + 0.9923)(z - 1.0002)z}$$

Following (18), the feedforward controller for 5MW Supergen wind turbine model is

$$FF_1(z) = \frac{B_1(z)}{V_1(z)} \quad (32)$$

If $P_{\omega_e\beta_c}(z)$ contains non-minimum phase zeros, the designed control system will be unstable. To deal with this problem, this research employs non-minimum phase zeros ignore (NPZ-Ignore) technique [46], in which all the nonminimum-phase zeros in the system model will be ignored [47, 48]. $FF_1(z)$ in (30) is then changed to

$$FF_1(z) = (2 \times 10^{-5}) \times \frac{(z + 9.1775)(z - 0.2666)(z + 0.1553)}{z^3} \quad (33)$$

Feedforward Controller for model II:

Similar to model I, the continuous transfer function $P_{\omega_e\beta_c}(s)$ is discretized to

$$P_{\omega_e\beta_c}(z) = \frac{B_2(z)}{W_2(z)} \quad (34)$$

with

$$\begin{aligned} B_2(z) = & -1.1095(z^2 - 1.9998z + 0.902) \\ & (z^2 - 2.0502z + 1.0546) \\ & (z^2 - 2z + 1.0005)(z^2 - 1.9996z + 1) \\ & (z + 1.1532)(z - 0.2523) \end{aligned} \quad (35)$$

$$\begin{aligned} W_2(z) = & (z^2 + 0.3156z + 0.624) \\ & (z^2 - 1.9796z + 0.9922) \\ & (z^2 - 1.9528z + 0.9570) \\ & (z^2 - 2.0022z + 0.9937) \\ & (z^2 - 1.9918z + 1.0067) \\ & (z - 0.9942) \end{aligned} \quad (36)$$

And

Chapter 4. Design of Feedforward Control

$$P_{\omega_e v_t}(z) = \frac{V_2(z)}{W_2(z)} \quad (37)$$

with

$$V_2(z) = (2.5921 \times 10^{-5})(z^2 - 1.9948z + 1.0004) \\ (z^2 - 1.9992z + 0.9997)(z^2 - 1.9992z + 0.9997) \quad (38)$$

$$(z + 9.1961)(z + 1.0895)(z - 0.2666)(z + 0.1549) \\ W_2(z) = (z^2 + 0.3156z + 0.624)(z^2 - 1.9796z + 0.9921) \\ (z^2 - 1.9528z + 0.9562)(z^2 - 2.0022z + 1.0028) \\ (z^2 - 1.9918z + 0.9923)(z - 1.0002) \quad (39)$$

A reduced-order feedforward controller is used for 5MW Supergen wind turbine linear model II as

$$FF_2(z) = (2.336 \times 10^{-5}) \times \frac{(z + 9.1961)(z - 0.2666)(z + 0.1549)}{z^3} \quad (40)$$

4.3 Simulation Results

In this subsection, the simulation results of feedforward control design for wind turbine model I and model II are discussed.

4.3.1 Simulation Results for Feedforward Controller I

The design of feedforward controller I is based on wind turbine linear model at operating point $\beta_0 = 0.15 \text{ deg}$, $\omega_0 = 120 \text{ rad/s}$, $U_0 = 12 \text{ m/s}$.

Chapter 4. Design of Feedforward Control

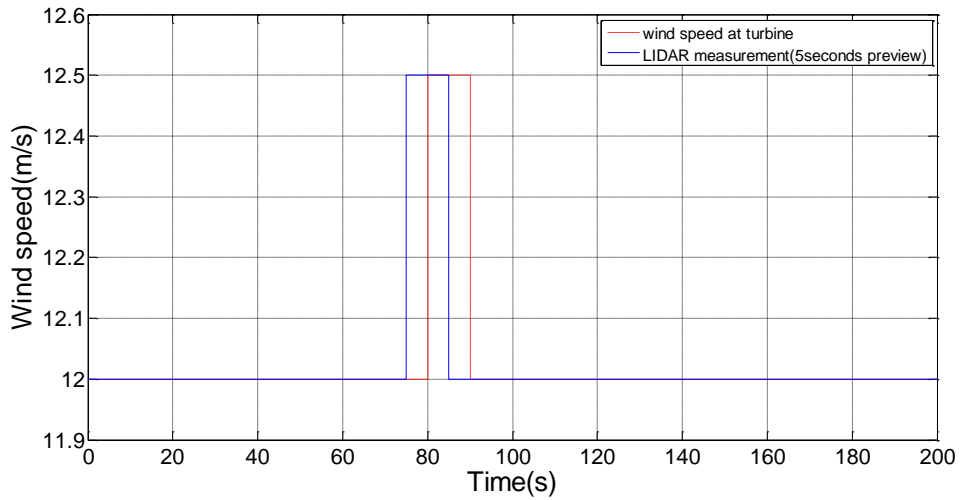


Figure 4.17: LIDAR measurement and turbine wind speed for model I

The simulation is conducted at a 12 m/s mean wind and the wind speed fluctuations are modelled by a set of small step signals added to the mean wind speed, see Figure 4.17. The turbine wind speed increases from 12m/s to 12.5m/s at 80s and reduces to 12m/s at 90s. The LIDAR measured wind speed is assumed to have 5 seconds preview ahead the turbine wind speed.

The factor 2×10^{-5} in equation (31) is noted as k_{FF1} . In order to fine tune the controller, a tuning factor $k_{FF2} = 2 \times 10^{-4}$ is introduced to the transfer function FF_1 . This tuning function can address modelling uncertainty to some extent.

As shown in the Figure 4.18 to 4.21, the influences of the feedforward controller are examined through plots of blade pitch demand, tower fore-aft acceleration, generator speed and the generated power. It can be seen from these figures that the feedforward term has almost no effect on the performance of the control system.

Chapter 4. Design of Feedforward Control

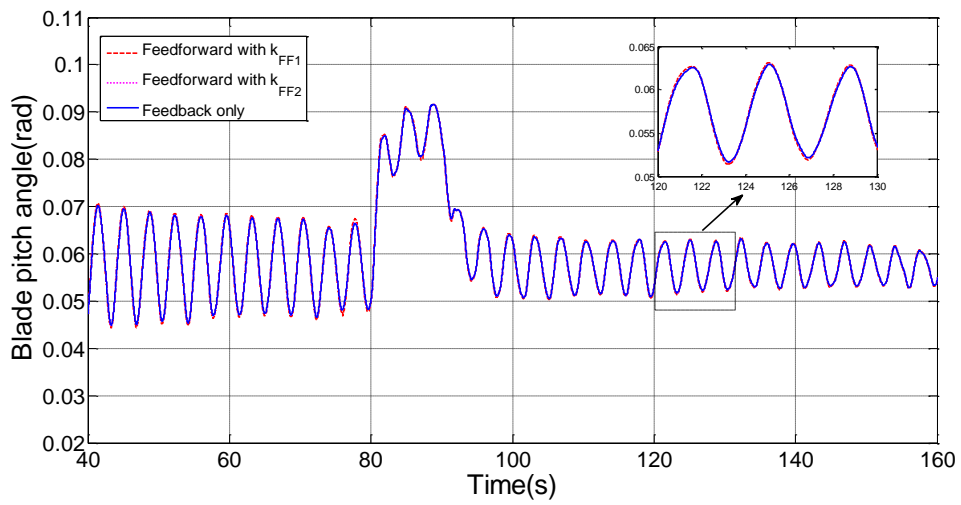


Figure 4.18: Comparison of the blade pitch angle before and after the addition of the feedforward controllers with k_{FF1} and k_{FF2}

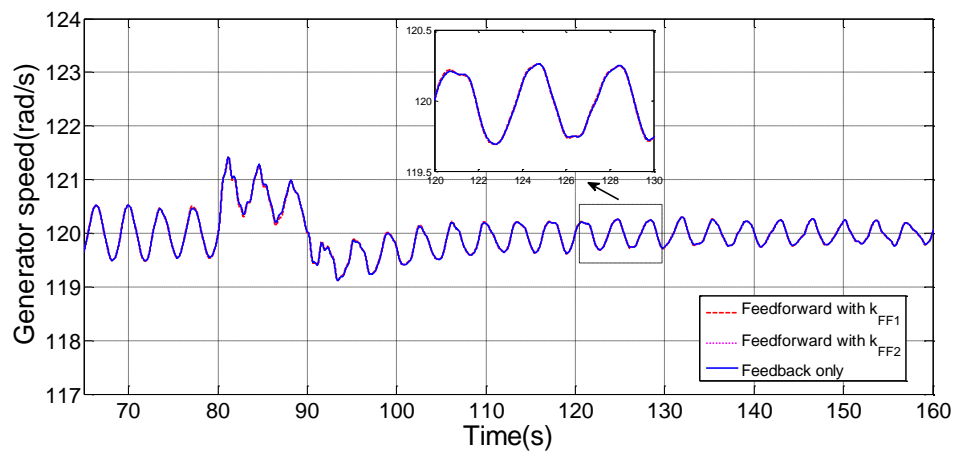


Figure 4.19: Comparison of the generator speed before and after the addition of the feedforward controllers with k_{FF1} and k_{FF2}

Chapter 4. Design of Feedforward Control

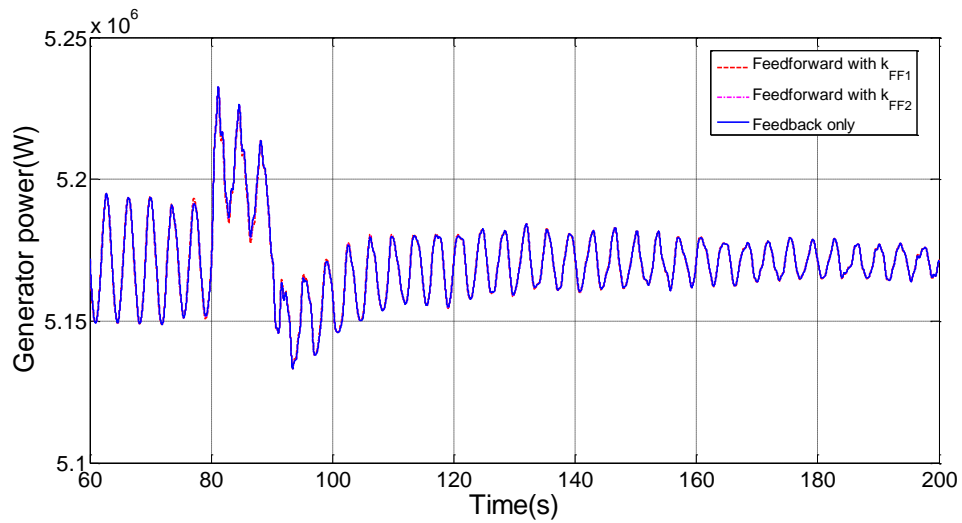


Figure 4.20: Comparison of the generator power before and after the addition of the feedforward controllers with k_{FF1} and k_{FF2}

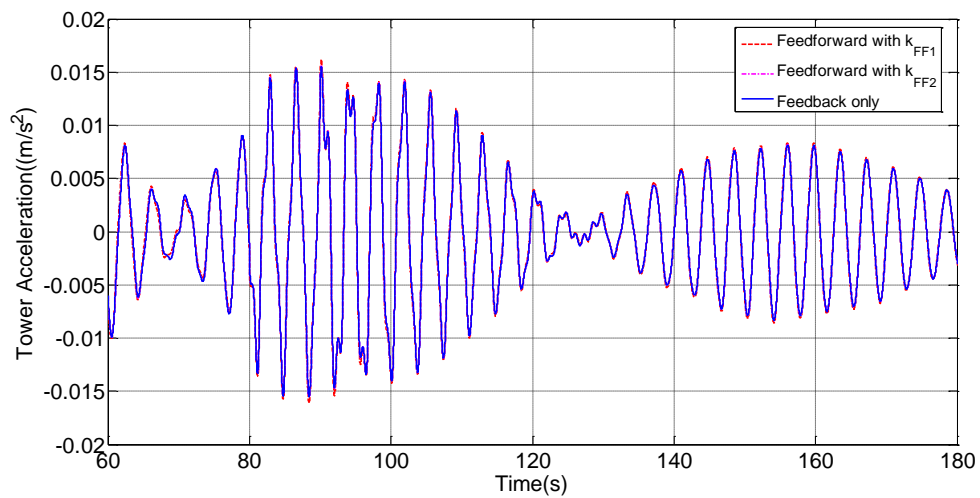
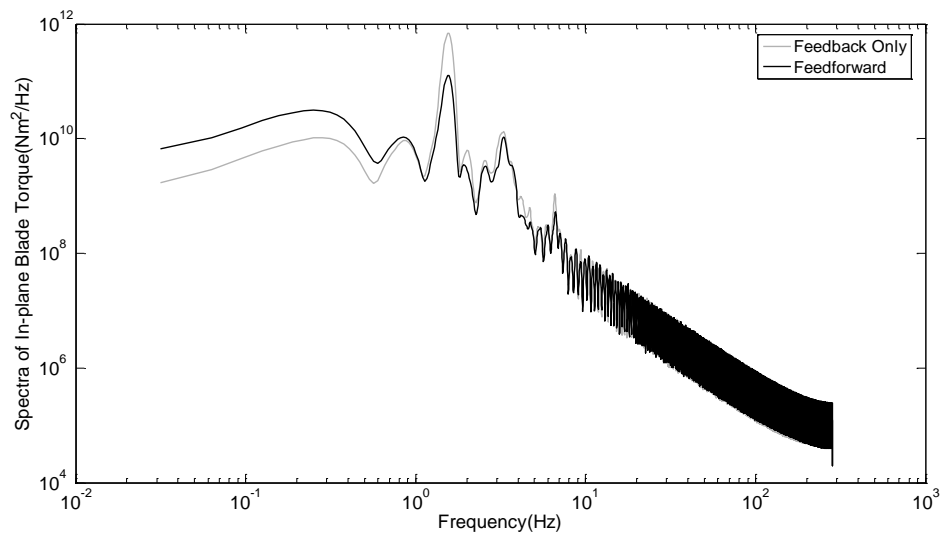


Figure 4.21: Comparison of the tower acceleration before and after the addition of the feedforward controllers with k_{FF1} and k_{FF2}

In order to further investigate the influences of the feedforward control loop to the wind turbine system. Some frequency domain simulation results are included in this research.

Chapter 4. Design of Feedforward Control

For the Supergen 5MW wind turbine model, the aerodynamic torque is modelled as a combination of in-plane and out-of-plane blade torque. The spectra of the in-plane and out-of-plane blade aerodynamic torques with and without the feedforward controller are depicted in Figure 4.22, in which k_{FF1} is the control factor. At frequencies higher than 1Hz and up to 5Hz, the in-plane blade torque is decreased. A reduction of the out-of-plane torque can be seen at frequencies higher than 0.6Hz. This indicates that the load which propagates from the aerodynamic load to the drive train is alleviated.



Chapter 4. Design of Feedforward Control

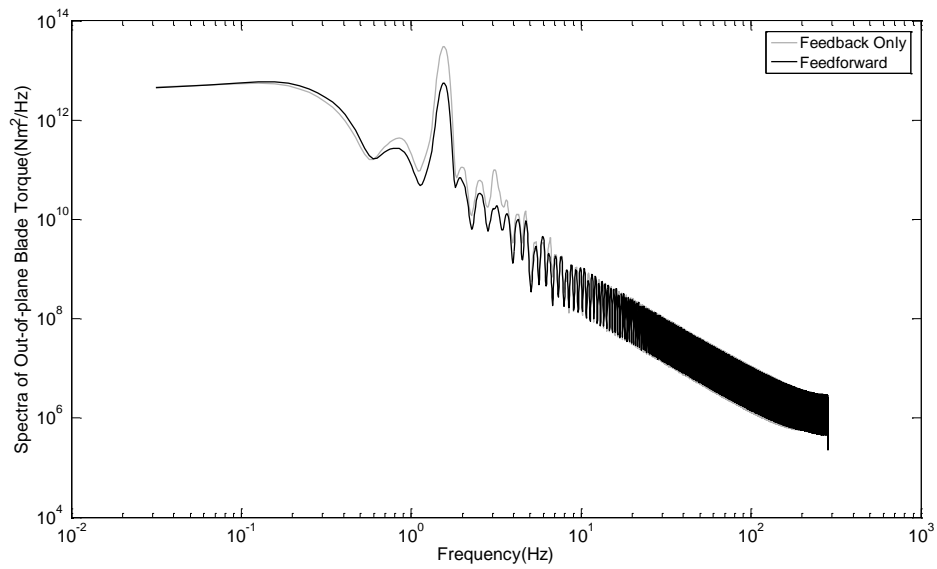


Figure 4.22: Comparisons of In-plane and Out-of-plane blade torques before and after the addition of the feedforward controller with k_{FF1}

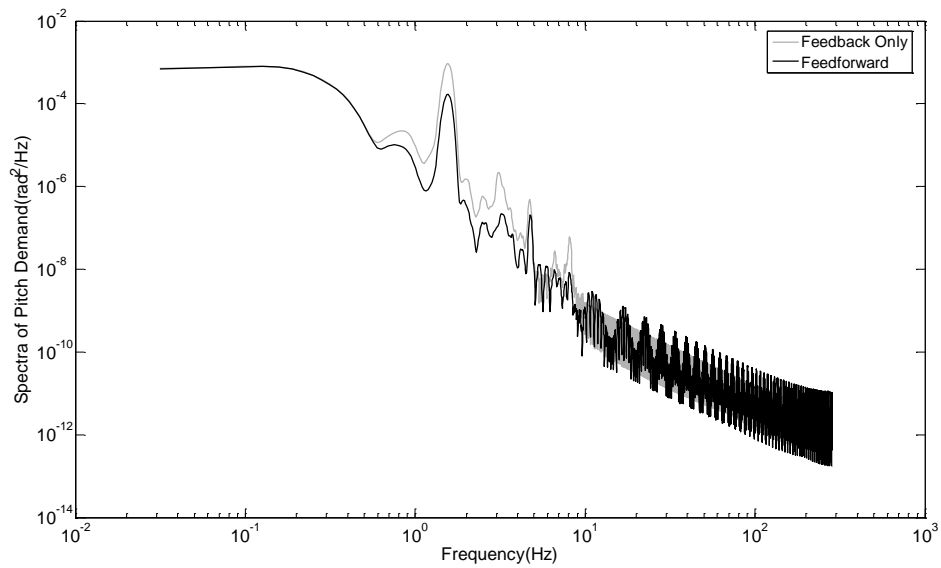


Figure 4.23: Spectra of the pitch demand for wind speed at 12m/s

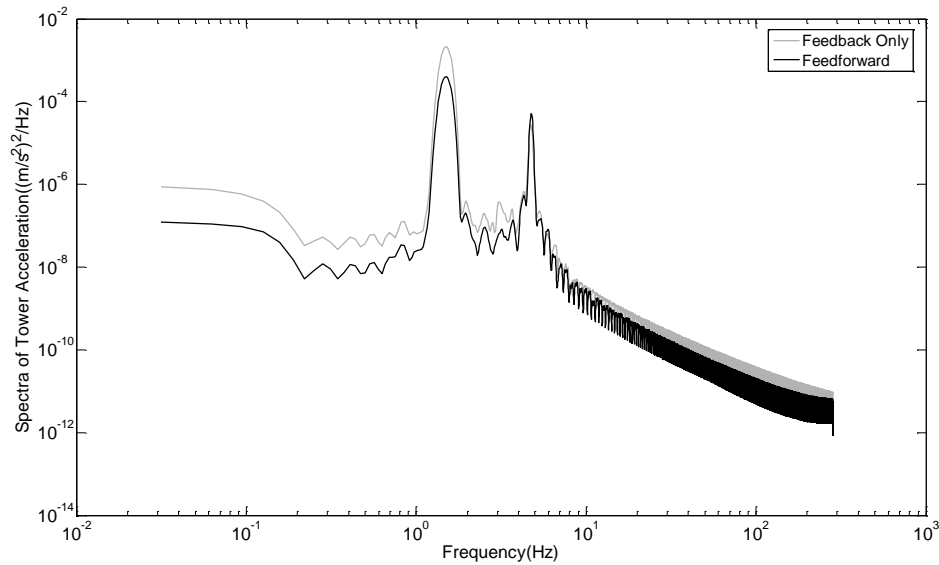


Figure 4.24: Spectra of the tower acceleration for wind speed at 12m/s

The spectra of pitch demand with and without feedforward controller are shown in Figure 4.23. Some pitch activity reductions can be seen at low frequencies and frequency range, 1Hz to 10Hz. The decrease in the pitch angle demand variations is able to expand the lifetime of pitch actuators. Figure 4.24 shows the comparison of the tower acceleration before and after the addition of feedforward control loop, fluctuation reductions can be seen at low frequencies.

In summary, the simulation results show that feedforward controller I has limited improvement to the loads reduction performance.

4.3.2 Simulation Results for Feedforward Controller II

Feedforward controller II is based on wind turbine linear model II at operating point $\beta_0 = 0.2113 \text{ deg}$, $\omega_0 = 120 \text{ rad/s}$, $U_0 = 16 \text{ m/s}$. The simulation is conducted at a 16 m/s mean wind combined with a set of small step signals (see Figure 4.25).

Chapter 4. Design of Feedforward Control

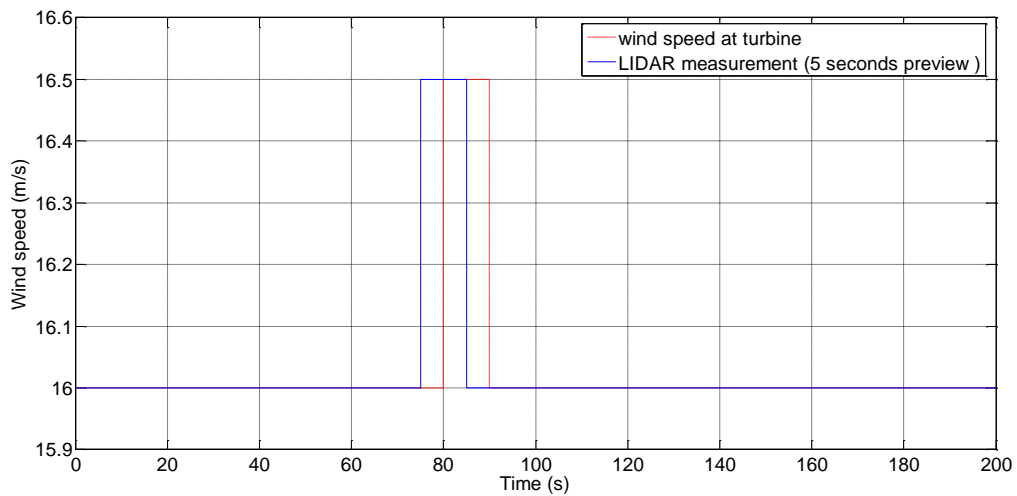


Figure 4.25: LIDAR measurement and turbine wind speed for controller II

The control factor 2.336×10^{-5} in equation (31) is noted as k_{FF3} and $k_{FF4} = 2.336 \times 10^{-4}$ is the tuning factor.

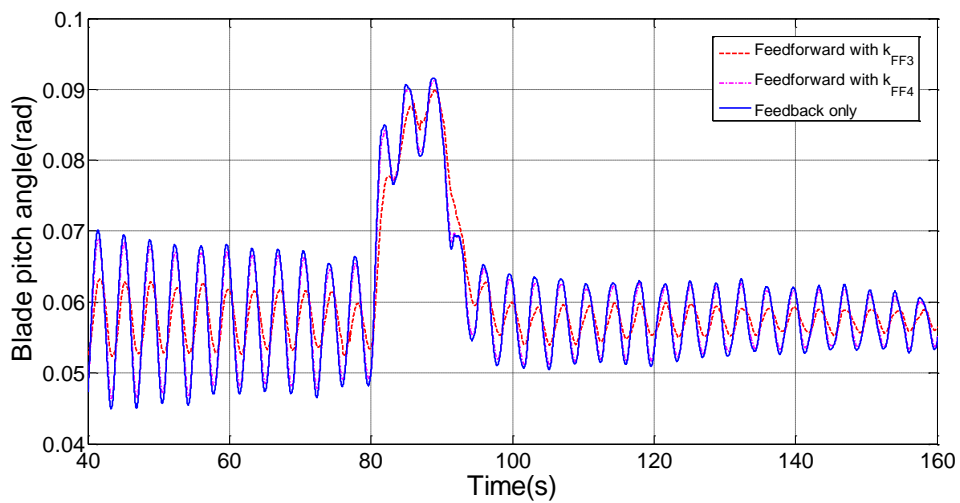


Figure 4.26: Comparison of the blade pitch angle between baseline controller and feedforward controllers with k_{FF3} and k_{FF4}

Chapter 4. Design of Feedforward Control

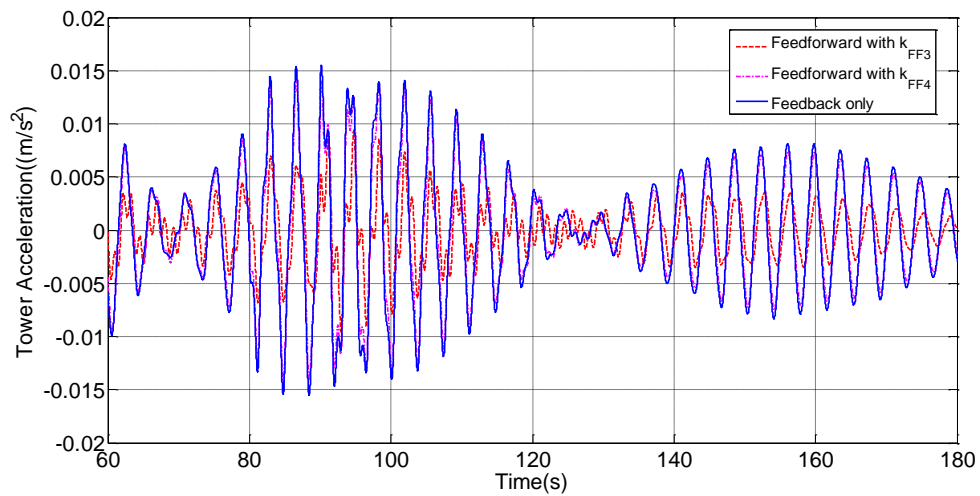


Figure 4.27: Comparison of the tower acceleration between baseline controller and feedforward controllers with k_{FF3} and k_{FF4}

In Figure 4.26 and Figure 4.27, the pitch demand and tower acceleration with and without the feedforward controllers are compared. The feedforward controller with fine-tuned factor $k_{FF4} = 2.336 \times 10^{-4}$ effectively reduces the fluctuations of the pitch demand and tower acceleration. Since the tower fore-aft acceleration is reduced, the oscillation of the tower is reduced and thereby the lifetime of the tower could be expanded. Moreover, the load that propagates from tower to drive train can also be alleviated.

Chapter 4. Design of Feedforward Control

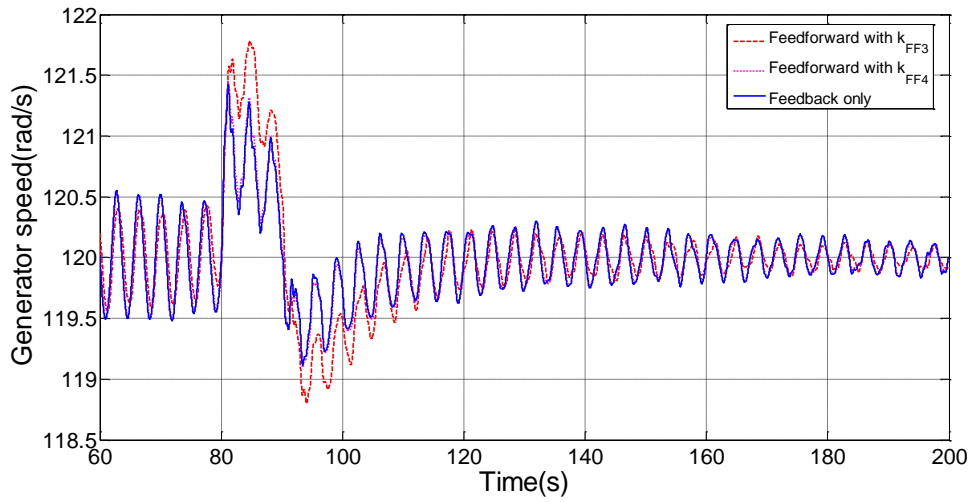


Figure 4.28: Comparison of the generator speed between baseline controller and feedforward controllers with k_{FF3} and k_{FF4}

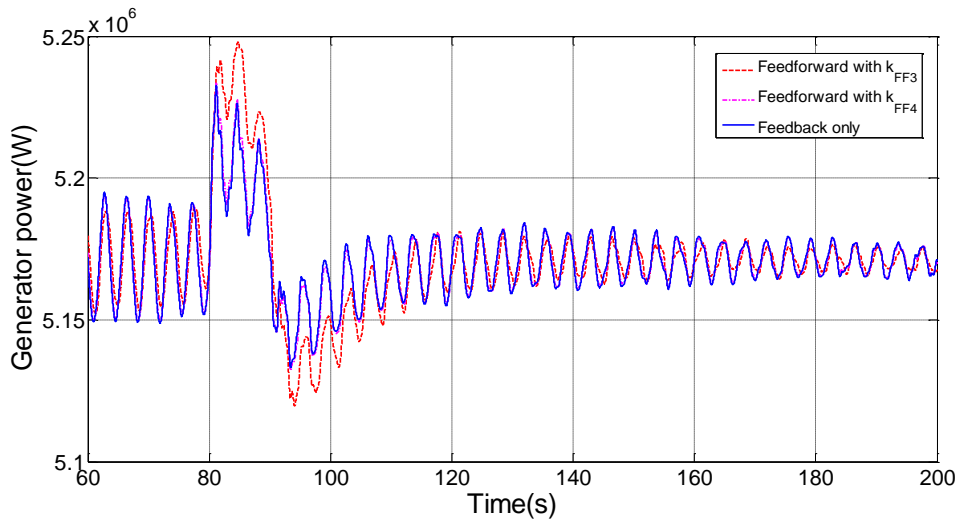


Figure 4.29: Comparison of the generator power between baseline controller and feedforward controllers with k_{FF3} and k_{FF4}

The generator speed and power with and without feedforward controllers are compared, see Figure 4.28 and Figure 4.29. The feedforward controller with $k_{FF4} = 2.336 \times 10^{-4}$ reduces the fluctuation of the generator speed in the whole time range except when the wind speed changes. The feedforward controllers affect the generator power in the same way.

Chapter 4. Design of Feedforward Control

It is evident from the previous results that the feedforward controller with tuned factor k_{FF4} is the most effective. It will be used as the default feedforward controller in the following simulation studies.

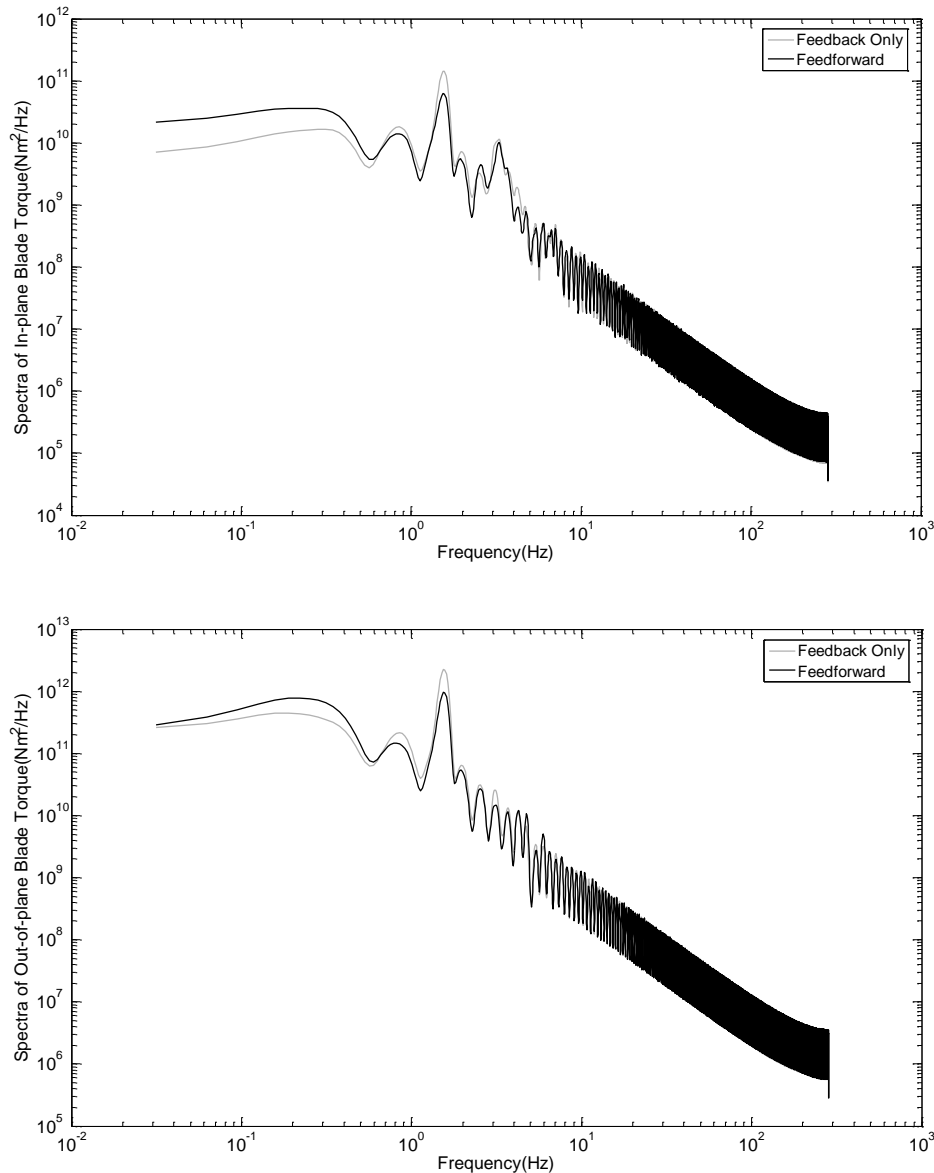


Figure 4.30: Comparisons of In-plane and Out-of-plane blade torques before and after the addition of the feedforward controller with k_{FF3}

The spectra of the in-plane and out-of-plane blade aerodynamic torques with and without the feedforward controller are depicted in Figure 4.30, where the

Chapter 4. Design of Feedforward Control

improvement in the in-plane torque is not evident at frequencies below 0.6Hz. However, a reduction can be seen at range from 0.6Hz to 10Hz. The feedforward term affects the out-of-plane torque in the same way.

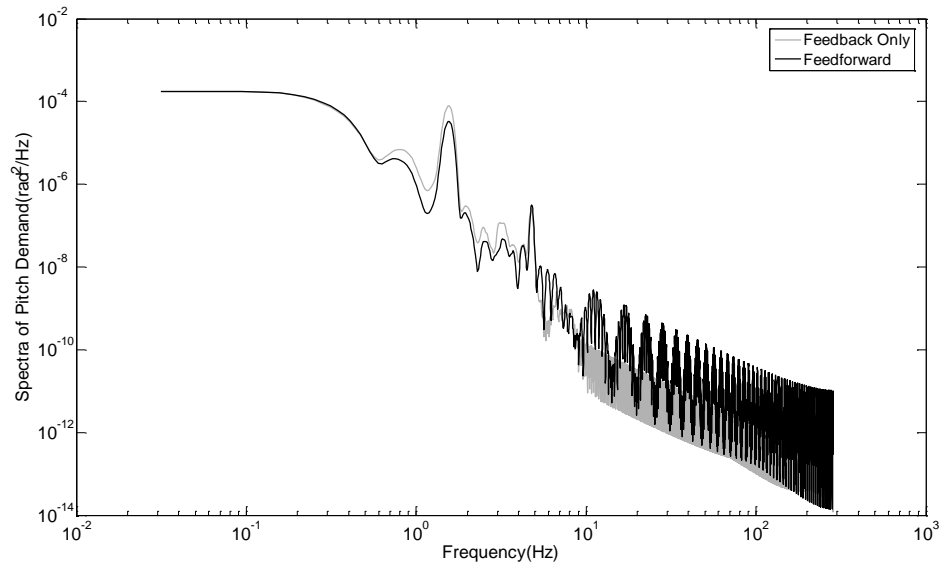


Figure 4.31: Spectra of the pitch demand for 16m/s wind speed

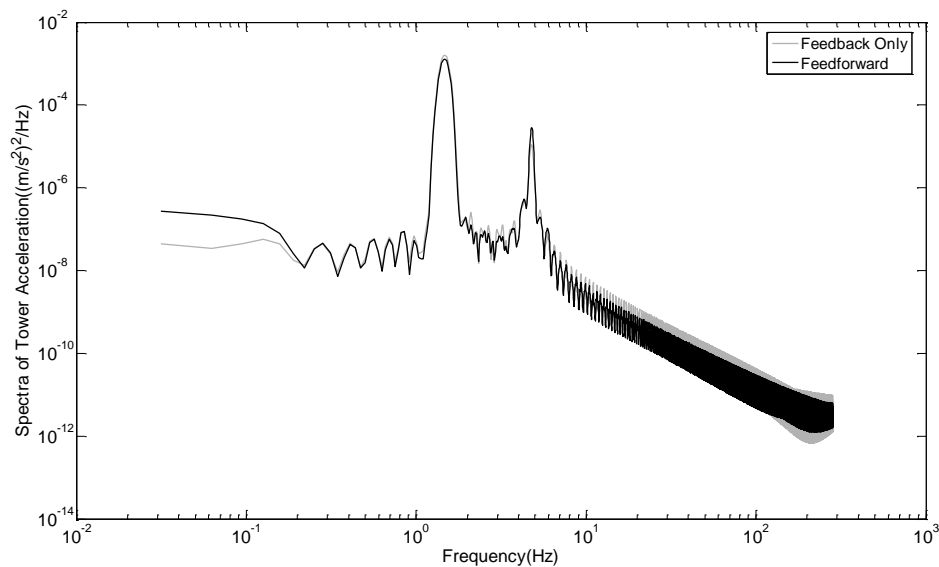


Figure 4.32: Spectra of the tower acceleration for 16m/s wind speed

Chapter 4. Design of Feedforward Control

Figure 4.31 shows the pitch demand spectra at wind speed 16m/s. The blade pitch activity is suppressed at low frequencies and some reductions appear at an intermediate frequency. The influences of the feedforward controller on the tower acceleration are not evident, see Figure 4.32.

The Bode plots of the open loop system with and without the feedforward control loop are included in this thesis. The Figure 4.33 to 4.35 show the bode diagrams from the wind speed disturbance to generator speed, hub torque and tower acceleration for wind speed of 16 m/s. The bode plots from pitch demand to various system outputs for wind speed of 16 m/s are depicted in the Figure 4.36 to 4.38. No effect can be identified from these simulation results when the feedforward controller is included. That is probably because of the design drawback of the Supergen wind turbine model. This problem will be dealt with in the future work.

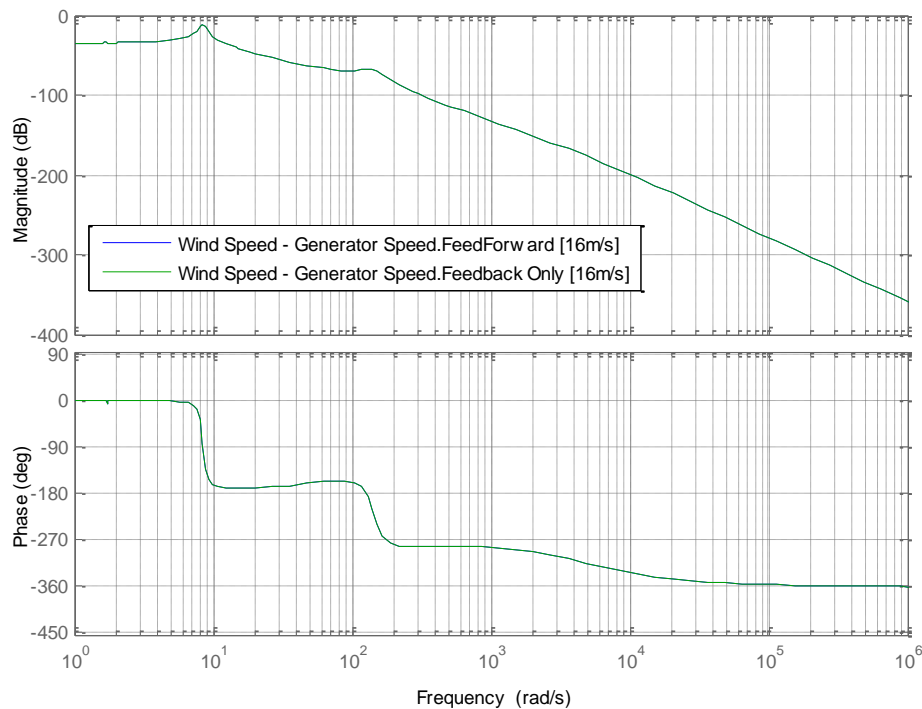


Figure 4.33: Open-loop Bode plot from Wind Speed to Generator Speed for 16m/s

Chapter 4. Design of Feedforward Control

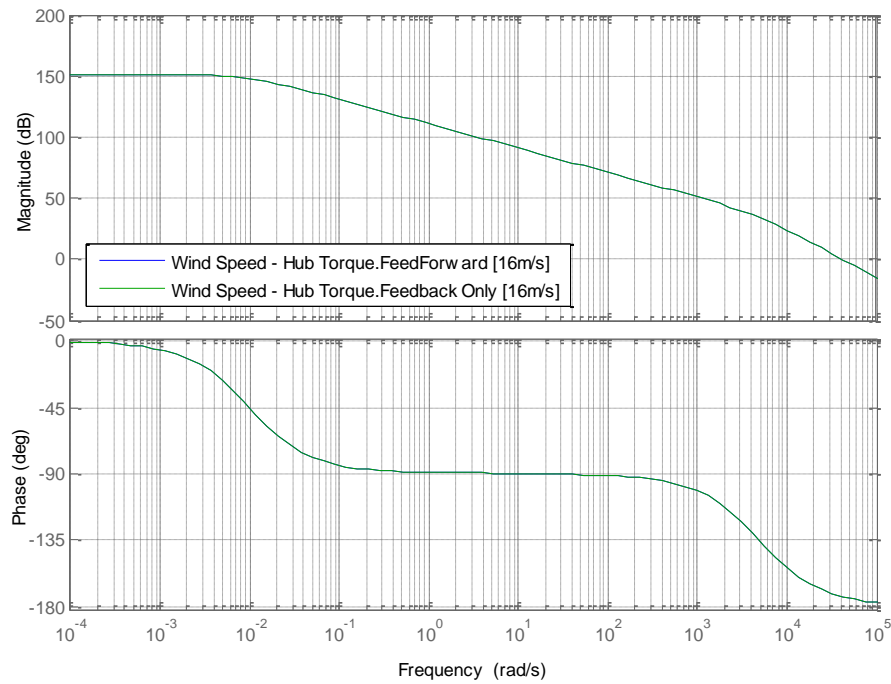


Figure 4.34: Open-loop Bode plot from Wind Speed to Hub Torque for 16m/s

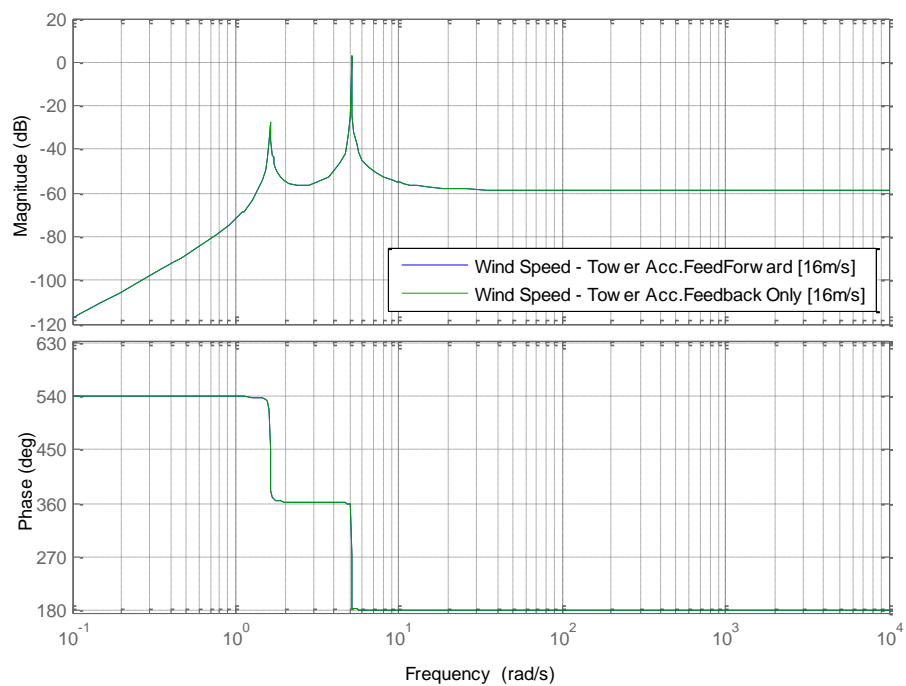


Figure 4.35: Open-loop Bode plot from Wind Speed to Tower Acceleration for 16m/s

Chapter 4. Design of Feedforward Control

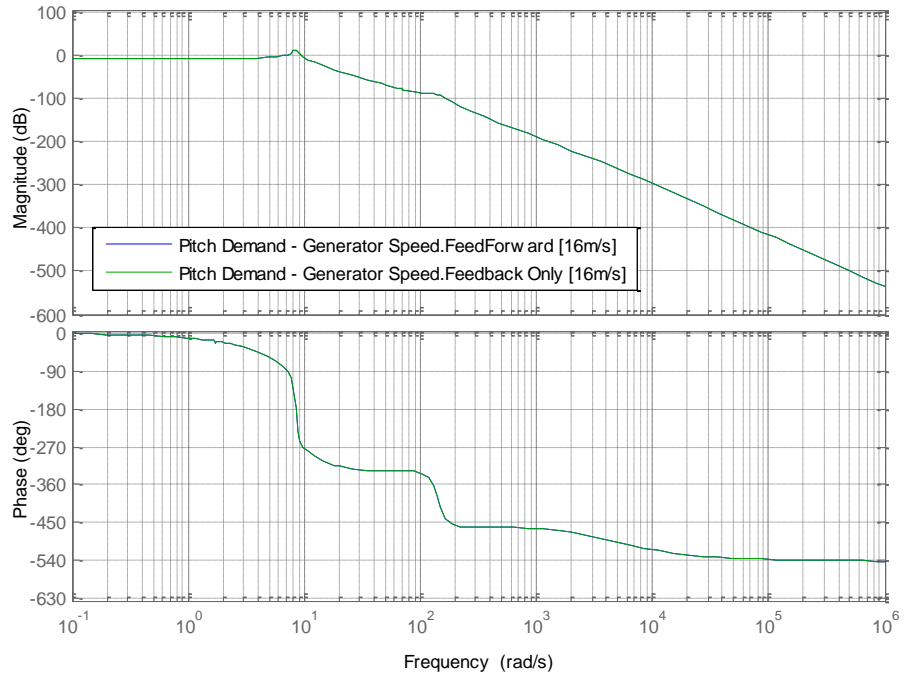


Figure 4.36: Open-loop Bode plot from Pitch Demand to Generator Speed for 16m/s

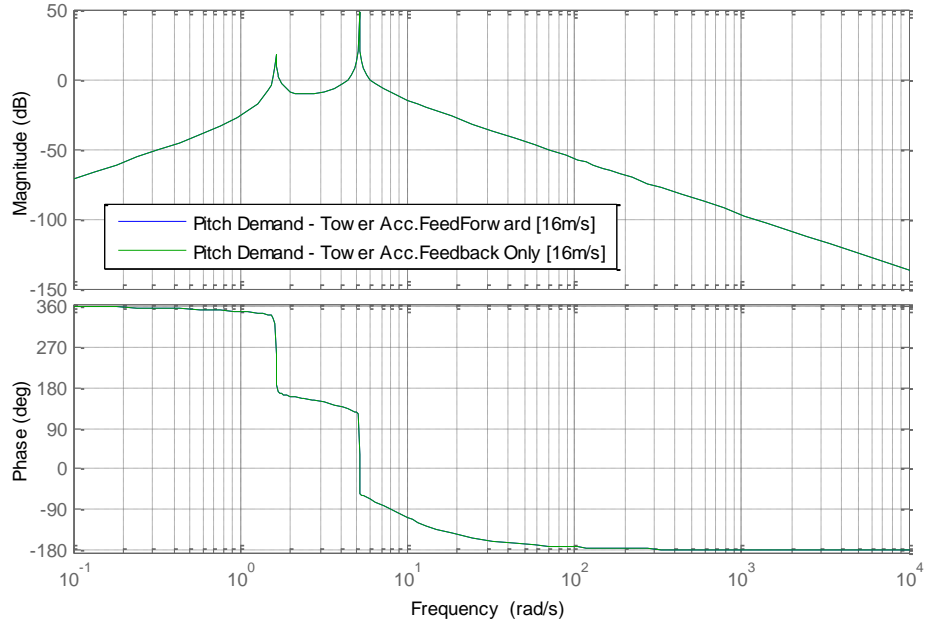


Figure 4.37: Open-loop Bode plot from Pitch Demand to Tower Acceleration for 16m/s

Chapter 4. Design of Feedforward Control

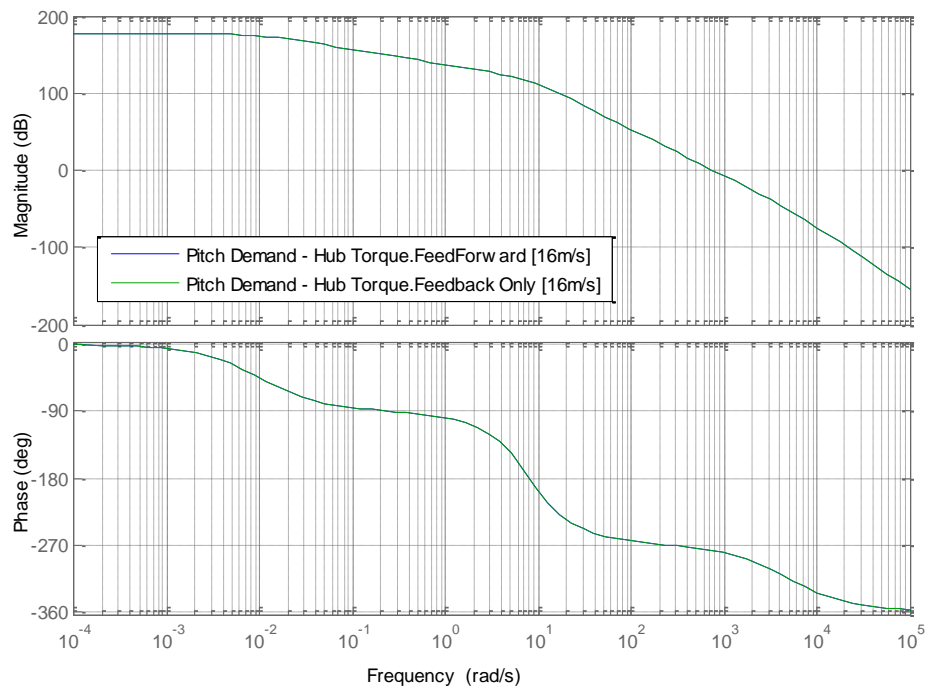


Figure 4.38: Open-loop Bode plot from Pitch Demand to Hub Torque for 16m/s

Chapter 5

Conclusions and Future Work

In this research, the control strategy for designing LIDAR-based feedforward controllers has been presented. A model-inversed feedforward pitch controller is combined with the baseline feedback pitch controller of the Supergen 5MW wind turbine model.

At first, LIDAR measurements and the turbine wind speed are simulated by Bladed. The cross spectrum between them and the auto spectrum of LIDAR wind speed measurements are studied. The results are used to develop the transfer function representing the evolution of LIDAR measurements across the distance from the measurement point to the wind turbine blades. At last, the feedforward controller is designed based on the Supergen linear wind turbine model and the transfer function.

The performance of the feedforward controller is evaluated at wind speed 12m/s and 16m/s respectively. The Simulink simulation study shows that the feedforward/feedback controller has achieved improved performance on reducing the fluctuations of the pitch angle demand and the tower acceleration without degrading the energy capture.

Based on the results reported in this thesis, recommendations for future research are:

Chapter 5. Conclusions and Future Work

1. Evaluate the performance of feedforward controller by calculating Damage Equivalent Loads (DEL), which can give more apparent comparisons between feedback control and feedforward/feedback control in load reduction.
2. Compare the feedforward/feedback control with individual pitch control and individual blade control in terms of load mitigation.
3. Model-inverse strategy is introduced to design the feedforward controller. Future work could be carried out to see if there are any other types of feedforward control design approaches, which are not strongly dependent on the wind turbine linear model.

References

- [1] Renewable UK, "The Impact of Wind Energy on UK Energy Dependence and Resilience," Available:<http://www.renewableuk.com/en/publications/index.cfm/Impact-of-Wind-Energy-on-UK-Energy-Dependence-and-Resilience>.
- [2] Renewable UK, "Wind Energy in the UK: State of the Industry Report 2014," Available: <http://www.renewableuk.com/en/publications/index.cfm/state-of-industry-report-2014>.
- [3] World Wind Energy Association. "World Wind Energy Report 2014," Available: http://www.wwindea.org/webimages/WWEA_half_year_report_2014.pdf.
- [4] W. E. Leithead and B. Connor, "Control of variable speed wind turbines: Design task," *International Journal of Control*, vol. 73, pp. 1189-1212, 2000.
- [5] F. D. Bianchi, H. De Battista, and R. J. Mantz, *Wind turbine control systems: principles, modelling and gain scheduling design*: Springer Science & Business Media, 2006.
- [6] http://www.bls.gov/green/wind_energy/.
- [7] E. N. Kirk Morgen, "Wind Turbine Foundation Behavior and Design Considerations," presented at the AWEA WINDPOWER Houston, 2008.
- [8] http://www.nrel.gov/wind/model_analysis.html.
- [9] <http://www.gl-qarradhasan.com/en/software/GHBladed.php>.
- [10] F. Dunne, L. Pao, A. D. Wright, B. Jonkman, and N. Kelley, "Combining standard feedback controllers with feedforward blade pitch control for load mitigation in wind turbines," in *Proc. 48th AIAA Aerospace Sciences Meeting, Orlando, FL, AIAA-2010-250*, 2010.
- [11] D. Schlipf, "LIDAR assisted collective pitch control," *UPWIND*, Technical Report Deliverable D 5.1.3, 2011.
- [12] W. V. Rietveld, "Wind speed feedforward control for a wind turbine using LIDAR " Master, Faculty of Mechanical, Maritime and Materials Engineering, Delft University of Technology, 2013.
- [13] International Electrotechnical Commission (IEC), "IEC 61400-1 3rd edition; Wind turbines-Design requirements," IEC, Switzerland, 2005.
- [14] E. Bossanyi, "Work Package 5 – Control systems: Final report," *UPWIND*, Technical Report Deliverable D 5.10, 2010.
- [15] E. A. Bossanyi, "The Design of closed loop controllers for wind turbines," *Wind Energy*, vol. 3, pp. 149-163, 2000.
- [16] W. E. Leithead and B. Connor, "Control of variable speed wind turbines: Dynamic models," *International Journal of Control*, vol. 73, pp. 1173-1188, 2000.
- [17] T. Burton, D. Sharpe, N. Jenkins, and E. Bossanyi, *Wind Energy Handbook*: John Wiley & Sons, 2001.

References

- [18] D. M. Robb, "Model based predictive control with application to renewable energy systems," PhD, University of Strathclyde, Glasgow, UK, 2000.
- [19] M. W. Jespersen, "Model Predictive LIDAR Control of Wind Turbines for Load Mitigation," Master, Aalborg University, 2011.
- [20] F. Dunne, L. Y. Pao, A. D. Wright, B. Jonkman, and N. Kelley, "Combining standard feedback controllers with feedforward blade pitch control for load mitigation in wind turbines," in *Proc. 48th AIAA Aerospace Sciences Meeting, Orlando, FL, AIAA-2010-250*, 2010.
- [21] E. A. Bossanyi, "Individual Blade Pitch Control for Load Reduction," *Wind Energy*, vol. 6, pp. 119–128, 2003.
- [22] E. A. Bossanyi, M. V. B. Bell, "Individual Blade Pitch Control with Integrated Control Algorithms and Load Measurement Instrumentation," presented at the AWEA Wind Power, Houston, Texas, 2008.
- [23] E. A. Bossanyi, "Further Load Reductions with Individual Pitch Controller," *Wind Energy*, vol. 8, pp. 481-485, 2005.
- [24] W. Leithead, V. Neilson, and S. Dominguez, "Alleviation of unbalanced rotor loads by single blade controllers," in *European Wind Energy Conference (EWEC 2009)*, 2009.
- [25] V. Neilson, "Individual Blade Control for Fatigue Load Reduction of Large-scaled Wind Turbines Theory and Modelling," Master, University of Strathclyde, 2010.
- [26] W. Leithead, V. Neilson, S. Dominguez, and A. Dutka, "A novel approach to structural load control using intelligent actuators," in *Control and Automation, 2009. MED'09. 17th Mediterranean Conference on*, 2009, pp. 1257-1262.
- [27] M. C. M. R. W. E. Leithead, "Drive-Train Characteristics of Constant Speed HAWT's: Part I - Representation by Simple Dynamic Models," *Wind Engineering*, vol. 20, 1996.
- [28] M. C. M. R. W. E. Leithead, "Drive-Train Characteristics of Constant Speed HAWT's: Part II - Simple Characterisation of Dynamics," *Wind Engineering*, vol. 20, 1996.
- [29] A. Stock, "Guide to the Supergen Controllers," Technical Report, University of Strathclyde, 2014.
- [30] I. Braña, "Turbine-Mounted Lidar: The pulsed lidar as a reliable alternative," Master, Department of Wind Energy, Gotland University, Gotland, 2011.
- [31] E. M. Steven Lang, "LIDAR and SODAR Measurements of Wind Speed and Direction in Upland Terrain for Wind Energy Purposes," *Remote Sensing*, 25 August 2011.
- [32] M. Harris, M. Hand, and A. Wright, "Lidar for turbine control," *National Renewable Energy Laboratory, Golden, CO, Report No. NREL/TP-500-39154*, 2006.
- [33] I. Antoniou, M. S. Courtney, H. Ejsing Jørgensen, T. Mikkelsen, S. V. Hunerbein, S. Bradley, *et al.*, "Remote sensing the wind using Lidars and Sodars," in *2007 European Wind Energy Conference and Exhibition*, 2007.
- [34] Zephir Ltd, "ZephIR Lidar Brochure," Ledbury, UK, 2014.
- [35] E. Simley and L. Pao, "Reducing lidar wind speed measurement error with optimal filtering," in *American Control Conference (ACC)*, 2013, pp. 621-627.
- [36] D. Schlipf, L. Y. Pao, and P. W. Cheng, "Comparison of feedforward and model predictive control of wind turbines using LIDAR," in *Proceedings of the Conference on Decision and Control*, Maui, USA, 2012.

References

- [37] F. Dunne, E. Simley, and L. Pao, "LIDAR Wind Speed Measurement Analysis and Feed-Forward Blade Pitch Control for Load Mitigation in Wind Turbines," *Golden, CO: National Renewable Energy Laboratory*, 2011.
- [38] E. A. Bossanyi, "Advanced controller research for multi-MW wind turbines in the UPWIND project," *Wind Energy*, 2012.
- [39] N. Wang, "LIDAR-based FX-RLS Feedforward Control For Wind Turbine Load mitigation," presented at the 2011 American Control Conference on O'Farrell Street, San Francisco, CA, USA, 2011.
- [40] M. Mirzaei, M. Soltani, N. K. Poulsen, and H. H. Niemann, "An MPC approach to individual pitch control of wind turbines using uncertain LIDAR measurements," in *Control Conference (ECC), 2013 European*, pp. 490-495.
- [41] L. C. Henriksen, N. K. Poulsen, and M. H. Hansen, "Nonlinear model predictive control of a simplified wind turbine," in *18th World Congress of the International Federation of Automatic Control*, 2011, pp. 551-556.
- [42] D. Schlipf, D. J. Schlipf, and M. Kühn, "Nonlinear model predictive control of wind turbines using LIDAR," *Wind Energy*, vol. 16, pp. 1107-1129, 2013.
- [43] N. Wang, "LIDAR-assisted Feedforward and Feedback Control Design for Wind Turbine Tower Load Mitigation and Power Capture Enhancement," Colorado School of Mines, 2013.
- [44] G. I. Taylor, "The spectrum of turbulence," *Proceedings of the Royal Society of London. Series A-Mathematical and Physical Sciences*, vol. 164, pp. 476-490, 1938.
- [45] N. Wang, K. E. Johnson, and A. D. Wright, "FX-RLS-based feedforward control for LIDAR-enabled wind turbine load mitigation," *Control Systems Technology, IEEE Transactions on*, vol. 20, pp. 1212-1222, 2012.
- [46] T. Masayoshi, "Zero Phase Error Tracking Algorithm for Digital Control," *Journal of Dynamic System, Measurement, and Control*, vol. 109, pp. 65-68, March 1987.
- [47] N. Wang, "LIDAR-assisted Feedforward and Feedback Control Design for Wind Turbine Tower Load Mitigation and Power Capture Enhancement," PhD, Colorado School of Mines, 2013.
- [48] R. C. Ko, M. C. Good, and S. K. Halgamuge, "Feedforward control strategies for high-speed contouring machine tools," in *Proc. of the Australian Conf. on Robotics and Automation*, 1999.

Appendix A

5MW Supergen Exemplar Wind Turbine Parameters

The parameters, which are necessary for the definition and formulation of the Simulink model, as well as the control models, of the exemplar 5MW Supergen wind turbine are listed below:

Parameters of the 5MW Supergen Exemplar Wind Turbine	
Rotor & Blade parameters	
Rotor radius [m]	$R = 63$
Effective blade length [m]	$L = 45$
Distance of the center of mass from the hub axis [m]	$R_c = 20.5$
One blade mass [Kg]	$M_{blade} = 17741$
One blade mass*3 [Kg]	$M_{bl} = M_{blade} * 3$
Hub height [m]	$h = 90$
Tower/Rotor cross-coupling inertia [Kg*m ²]	$J_c = R_c * h * M_{bl}$
Flap natural frequency [rad/s]	$w_f = 4.1595$
Rotor inertia [Kg*m ²]	$J = 3.53715e+007$
Blade flapwise stiffness [Nm/rad]	$K_f = w_f^2 * J$
Edge natural frequency [rad/s]	$w_e = 6.7984$
Blade edgewise stiffness [Nm/rad]	$K_e = w_e^2 * J$

Appendix A. 5MW Supergen Exemplar Wind Turbine Parameters

Rotor and nacelle mass [Kg]	$Mr_n = 97961$
Tower parameters	
Tower fore-aft inertia [Kg*m ²]	$Jt = h^2*(Mr_n - Mbl)$
Tower fore-aft frequency [rad/s]	$w_t = 1.7467$
Tower fore-aft damping	$Bt_param = 0.01$
Tower fore-aft damping moment	$Bt = 2*Bt_param*w_t*Jt$
Tower fore-aft stiffness [Nm/rad]	$Kt = w_t^2*Jt$
Tower side-side natural frequency [rad/s]	$w_{ts} = 1.7593$
Tower side-side inertia [Kg*m ²]	$Jts = h^2*Mr_n$
Tower side-side stiffness [Nm/rad]	$Kts = w_{ts}^2*Jts$
Tower side-side damping	$Bts_param = 0.01$
Tower side-side damping moment	$Bts = 2*Bts_param*w_{ts}*Jts$
Coefficient to adjust tower/nacelle displacement	$Ka = 120$
Pitch Actuator parameters	
Pitch actuator transfer function	$G_{pa}(s) = \frac{64}{s^2 + 11.2s + 64}$
Operational parameters	
Minimum generator speed in generation mode [rad/s]	$WMIN = 70$
Maximum generator speed in generation mode [rad/s]	$WMAX = 120$
Cut in wind speed [m/s]	$WCUTIN = 4$
Cut out wind speed [m/s]	$WCUTOUT = 25$
Nominal generator torque	$TQSET = 46372.7$
Minimum pitch angle [deg]	$PITMIN = 0$

Appendix A. 5MW Supergen Exemplar Wind Turbine Parameters

Maximum pitch angle [deg]	PITMAX = 30
Sampling time [s]	sample_time = 0.01
Air density [Kg/m ³]	rho = 1.225
Drive-train parameters	
Hub inertia [Kg*m ²]	ILs = 115926
Low speed shaft damping[Nms/rad]	gls = 150000
High speed shaft damping[Nms/rad]	ghs = 5
Low speed shaft stiffness [Nm/rad]	KLsb = 4.45e+008
Low speed shaft material damping[Nms/rad]	g1s = 4.2e+006
High speed shaft material damping[Nms/rad]	g2s = 1000
High speed shaft stiffness [Nm/rad]	KHs = 1e+08
Gearbox ratio	N=n = 97
High speed shaft inertia [Kg*m ²]	J_Hs = 5
Generator inertia [Kg*m ²]	J_gen = 534.116
Drive-train efficiency below rated	EtaFL = 1
Drive-train efficiency above rated	EtaVS = 1
High speed shaft + generator inertia [Kg*m ²]	IHs = J_Hs+J_gen

Appendix B

5MW Wind Turbine Linear Model

B.1 5MW Wind Turbine State-space Model

The linear model of 5MW wind turbine is stated as

$$\begin{cases} \dot{x} = Ax + Bu \\ y = Cx + Du \end{cases}$$

B.1.1 Linear Model I

Linear model I is the wind turbine model linearised at operating point

$$\beta_0 = 0.15 \text{ deg}, \omega_0 = 120 \text{ rad/s}, U_0 = 12 \text{ m/s}.$$

B.1.1.1 When the pitch angle is the input and the generator speed is the output

Matrix A

$$A = \begin{bmatrix} 0 & 0 & 0 & 16 & 0 & 0 & -128 & 0 & 0 & 0 & 0 & 0 \\ 0 & 0 & 0 & 0 & 16 & 0 & 0 & 0 & 0 & 0 & 0 & 0 \\ 0 & 0 & 0 & 0 & 0 & 16 & 0 & 0 & 0 & 0 & 0 & 0 \\ -3.09 & 0.53 & -0.13 & -0.12 & -2.36 & -1.18 & 0 & 0 & 0 & 0 & 0 & 0 \\ 0.13 & -1.46 & 0.38 & -0.07 & -3.83 & -1.91 & 0 & 0 & 0 & 0 & 0 & 0 \\ -0.01 & 0.12 & -0.22 & 0 & 0.61 & 0.01 & 0 & 0 & 0 & 0 & 0 & 0 \\ 129.5 & -22.15 & 5.54 & 0 & 0 & 0 & -26.34 & -50.03 & 0.19 & 0 & -8.66e + 03 & 4.13 \\ 0 & 0 & 0 & 0 & 0 & 0 & 36.68 & -32.70 & -0.28 & 0 & 1.27e + 04 & -6.05 \\ 0 & 0 & 0 & 0 & 0 & 0 & 0.13 & 0.26 & 0.03 & -1.52 & 44.88 & -0.02 \\ 0 & 0 & 0 & 0 & 0 & 0 & 0 & 0 & 2 & 0 & 0 & 0 \\ 0 & 0 & 0 & 0 & 0 & 0 & 8.92e + 03 & 1.78e + 04 & -69 & 0 & -6.91e + 06 & -1.47e + 03 \\ 0 & 0 & 0 & 0 & 0 & 0 & 3.47 & 6.93 & 0.03 & 0 & 1.2e + 03 & -0.58 \end{bmatrix}$$

Matrix B

$$B = \begin{bmatrix} 0 \\ 0 \\ 0 \\ -0.64 \\ -8.11 \\ 0.13 \\ -104.56 \\ 0 \\ 0 \\ 0 \\ 0 \\ 0 \\ 0 \\ 0 \end{bmatrix}$$

Matrix C

$$C = [0 \ 0 \ 0 \ 0 \ 0 \ 0 \ 0 \ 0 \ 0 \ 0 \ 0 \ 0 \ 0 \ 32]$$

Matrix D

$$D = 0$$

B.1.1.2 When the wind speed is the input and the generator speed is the output

$$A = \begin{bmatrix} 0 & 0 & 0 & 16 & 0 & 0 & -128 & 0 & 0 & 0 & 0 & 0 & 0 \\ 0 & 0 & 0 & 0 & 16 & 0 & 0 & 0 & 0 & 0 & 0 & 0 & 0 \\ 0 & 0 & 0 & 0 & 0 & 16 & 0 & 0 & 0 & 0 & 0 & 0 & 0 \\ -3.1 & 0.5 & -0.1 & -0.1 & -2.4 & -1.2 & 0 & 0 & 0 & 0 & 0 & 0 & 0 \\ 0.1 & -1.5 & 0.4 & 0 & -3.8 & -1.9 & 0 & 0 & 0 & 0 & 0 & 0 & 0 \\ 0 & 0.1 & -0.2 & 0 & 0.6 & 0 & 0 & 0 & 0 & 0 & 0 & 0 & 0 \\ 129.5 & -22.15 & 5.54 & 0 & 0 & 0 & -26.34 & -50.03 & 0.19 & 0 & -8.66e + 03 & 4.13 & 0 \\ 0 & 0 & 0 & 0 & 0 & 0 & 36.68 & -32.7 & -0.28 & 0 & 1.27e + 04 & -6.05 & 0 \\ 0 & 0 & 0 & 0 & 0 & 0 & 0.13 & 0.26 & -0.03 & -1.52 & 44.88 & -0.02 & 0 \\ 0 & 0 & 0 & 0 & 0 & 0 & 0 & 0 & 1.97 & 0 & 0 & 0 & 0 \\ 0 & 0 & 0 & 0 & 0 & 0 & 8.92e + 03 & 1.78e + 04 & -69.98 & 0 & -6.91e + 06 & -1.47e + 03 & 0 \\ 0 & 0 & 0 & 0 & 0 & 0 & 3.47 & 6.93 & -0.03 & 0 & 1.2e + 03 & -0.58 & 0 \end{bmatrix}$$

Appendix B. 5MW Wind Turbine Linear Model

Matrix B

$$B = \begin{bmatrix} 0 \\ 0 \\ 0 \\ 0.1051 \\ 0.1700 \\ -0.0027 \\ 0 \\ 0 \\ 0 \\ 0 \\ 0 \\ 0 \\ 0 \end{bmatrix}$$

Matrix C

$$C = [0 \ 0 \ 0 \ 0 \ 0 \ 0 \ 0 \ 0 \ 0 \ 0 \ 0 \ 0 \ 32]$$

Matrix D

$$D = 0$$

B.1.2 Linear Model II

Linear model II is the wind turbine model linearised at operating point

$$\beta_0 = 0.2113 \text{ deg}, \omega_0 = 120 \text{ rad/s}, U_0 = 16 \text{ m/s}$$

B.1.2.1 When the pitch angle is the input and the generator speed is the output

Matrix A

$$A = \begin{bmatrix} 0 & 0 & 0 & 16 & 0 & 0 & -128 & 0 & 0 & 0 & 0 & 0 \\ 0 & 0 & 0 & 0 & 16 & 0 & 0 & 0 & 0 & 0 & 0 & 0 \\ 0 & 0 & 0 & 0 & 0 & 16 & 0 & 0 & 0 & 0 & 0 & 0 \\ -3.06 & 0.36 & -0.18 & -0.19 & -1.28 & -1.28 & 0 & 0 & 0 & 0 & 0 & 0 \\ 0.36 & -1.5 & 0.77 & -0.38 & -3.75 & -3.74 & 0 & 0 & 0 & 0 & 0 & 0 \\ -0.01 & 0.06 & -0.22 & 0 & 0.03 & 0.01 & 0 & 0 & 0 & 0 & 0 & 0 \\ 127.93 & -22.12 & 7.56 & 0 & 0 & 0 & -26.34 & -50.03 & 0.19 & 0 & -8.66e + 03 & 4.13 \\ 0 & 0 & 0 & 0 & 0 & 0 & 36.68 & -32.7 & -0.28 & 0 & 1.27e + 04 & -6.05 \\ 0 & 0 & 0 & 0 & 0 & 0 & 0.13 & 0.26 & 0.03 & -1.52 & 44.88 & -0.02 \\ 0 & 0 & 0 & 0 & 0 & 0 & 0 & 0 & 1.97 & 0 & 0 & 0 \\ 0 & 0 & 0 & 0 & 0 & 0 & 8.92e + 03 & 1.78e + 04 & -68.98 & 0 & -6.91e + 06 & -1.47e + 03 \\ 0 & 0 & 0 & 0 & 0 & 0 & 3.47 & 6.93 & 0.03 & 0 & 1.2e + 03 & -0.58 \end{bmatrix}$$

Matrix B

$$B = \begin{bmatrix} 0 \\ 0 \\ 0 \\ 0.11 \\ 0.17 \\ 0 \\ 0 \\ 0 \\ 0 \\ 0 \\ 0 \\ 0 \\ 0 \\ 0 \end{bmatrix}$$

Matrix C

$$C = [0 \ 0 \ 0 \ 0 \ 0 \ 0 \ 0 \ 0 \ 0 \ 0 \ 0 \ 0 \ 0 \ 32]$$

Matrix D

$$D = 0$$

B.1.2.2 When the wind speed is the input and the generator speed is the output

Matrix A

$$A = \begin{bmatrix} 0 & 0 & 0 & 16 & 0 & 0 & -128 & 0 & 0 & 0 & 0 & 0 \\ 0 & 0 & 0 & 0 & 16 & 0 & 0 & 0 & 0 & 0 & 0 & 0 \\ 0 & 0 & 0 & 0 & 0 & 16 & 0 & 0 & 0 & 0 & 0 & 0 \\ -3.09 & 0.53 & -0.13 & -0.12 & -2.36 & -1.18 & 0 & 0 & 0 & 0 & 0 & 0 \\ 0.13 & -1.46 & 0.38 & -0.07 & -3.83 & -1.91 & 0 & 0 & 0 & 0 & 0 & 0 \\ -0.01 & 0.12 & -0.22 & 0 & 0.61 & 0.01 & 0 & 0 & 0 & 0 & 0 & 0 \\ 127.93 & -15.12 & 7.56 & 0 & 0 & 0 & -26.34 & -50.03 & 0.19 & 0 & -8.66e + 03 & 4.13 \\ 0 & 0 & 0 & 0 & 0 & 0 & 36.68 & -32.7 & -0.28 & 0 & 1.27e + 04 & -6.05 \\ 0 & 0 & 0 & 0 & 0 & 0 & 0.13 & 0.26 & -0.03 & -1.52 & 44.88 & -0.02 \\ 0 & 0 & 0 & 0 & 0 & 0 & 0 & 0 & 1.97 & 0 & 0 & 0 \\ 0 & 0 & 0 & 0 & 0 & 0 & 8.92e + 03 & 1.78e + 04 & -68.98 & 0 & -6.91e + 06 & -1.47e + 03 \\ 0 & 0 & 0 & 0 & 0 & 0 & 3.47 & 6.93 & -0.03 & 0 & 1.2e + 03 & -0.58 \end{bmatrix}$$

Appendix B. 5MW Wind Turbine Linear Model

Matrix B

$$B = \begin{bmatrix} 0 \\ 0 \\ 0 \\ 0.11 \\ 0.33 \\ 0 \\ 0 \\ 0 \\ 0 \\ 0 \\ 0 \\ 0 \\ 0 \end{bmatrix}$$

Matrix C

$$C = [0 \ 0 \ 0 \ 0 \ 0 \ 0 \ 0 \ 0 \ 0 \ 0 \ 0 \ 0 \ 0 \ 32]$$

Matrix D

$$D = 0$$

B.2 5MW Wind Turbine Transfer Function Model

B.2.1 Transfer Functions for Wind Turbine Model I

$$P_{\omega_e \beta_c}(s) = \frac{B_1(s)}{W_1(s)}$$

with

$$\begin{aligned} B_1(s) = & -1.161e04 s^{10} - 1.161e11 s^9 - 1.276e13 s^8 - 5.632e13 s^7 \\ & - 7.847e14 s^6 + 1.089e15 s^5 - 2.216e16 s^4 + 9.408e15 s^3 \\ & - 1.119e17 s^2 + 1.692e16 s - 1.565e17 \end{aligned}$$

and

$$\begin{aligned} W_1(s) = & s^{12} + 6.914e06 s^{11} + 2.927e08 s^{10} + 1.434e11 s^9 + 6.822e11 s^8 \\ & + 1.612e13 s^7 + 5.319e13 s^6 + 3.662e14 s^5 + 3.882e14 s^4 \\ & + 1.752e15 s^3 + 7.91e14 s^2 + 2.38e15 s + 2.64e14 \end{aligned}$$

$$P_{\omega_e v_t}(s) = \frac{V_1(s)}{W_1(s)}$$

with

$$\begin{aligned} V_1(s) = & 1.746e04 s^8 + 1.746e11 s^7 + 1.85e13 s^6 + 7.056e12 s^5 \\ & + 7.117e14 s^4 + 6.318e13 s^3 + 3.717e15 s^2 + 1.295e14 s \\ & + 5.245e15 \end{aligned}$$

and

$$\begin{aligned} W_1(s) = & s^{12} + 6.914e06 s^{11} + 2.927e08 s^{10} + 1.434e11 s^9 + 6.822e11 s^8 \\ & + 1.612e13 s^7 + 5.319e13 s^6 + 3.662e14 s^5 + 3.882e14 s^4 \\ & + 1.752e15 s^3 + 7.91e14 s^2 + 2.38e15 s + 2.64e14 \end{aligned}$$

B.2.2 Transfer Functions for Wind Turbine Model II

$$P_{\omega_{g.e}\beta}(s) = \frac{B_2(s)}{W_2(s)}$$

with

$$\begin{aligned} B_2(s) = & -9847 s^{10} - 9.847e10 s^9 - 1.082e13 s^8 - 4.923e13 s^7 - 8.305e14 s^6 \\ & + 7.929e14 s^5 - 2.84e16 s^4 + 6.861e15 s^3 - 1.473e17 s^2 + 1.215e16 s \\ & - 2.079e17 \end{aligned}$$

And

$$\begin{aligned} W_2(s) = & s^{12} + 6.914e06 s^{11} + 2.926e08 s^{10} + 1.42e11 s^9 + 6.744e11 s^8 \\ & + 1.598e13 s^7 + 5.274e13 s^6 + 3.649e14 s^5 + 4.015e14 s^4 \\ & + 1.748e15 s^3 + 8.836e14 s^2 + 2.376e15 s + 4.105e14 \end{aligned}$$

$$P_{\omega_{g.e}\beta}(s) = \frac{V_2(s)}{W_2(s)}$$

With

$$\begin{aligned} V_2(s) = & 1.692e04 s^8 + 1.692e11 s^7 + 1.793e13 s^6 + 7.428e12 s^5 \\ & + 7.59e14 s^4 + 6.803e13 s^3 + 4.012e15 s^2 + 1.404e14 s \\ & + 5.688e15 \end{aligned}$$

And

$$\begin{aligned} W_2(s) = & s^{12} + 6.914e06 s^{11} + 2.926e08 s^{10} + 1.42e11 s^9 + 6.744e11 s^8 \\ & + 1.598e13 s^7 + 5.274e13 s^6 + 3.649e14 s^5 + 4.015e14 s^4 \\ & + 1.748e15 s^3 + 8.836e14 s^2 + 2.376e15 s + 4.105e14 \end{aligned}$$

Appendix C

Matlab Code for the Project

C.1 Code for Cross Correlation

```
%Load the wind speed data from Bladed

load('crosscorrelaton.mat')

%Input wind speed data

x1=ww1_0
x2=ww2_7
x3=ww3_14
x4=ww_21(:,1)
x5=ww_21(:,2)
x6=ww_21(:,3)

%Detrend wind speed data

x1=detrend(x1);
x2=detrend(x2);
x3=detrend(x3);
x4=detrend(x4);
x5=detrend(x5);
x6=detrend(x6);

%Maintain effective data
```

Appendix C. Matlab Code for the Project

```
xx1=x1(200:end);
xx2=x2(200:end);
xx3=x3(200:end);
xx4=x4(200:end);
xx5=x5(200:end);
xx6=x6(200:end);

%Calculate cross correlation

[c_ww1,lags1] = xcorr(xx1,xx2,'coeff');
[c_ww2,lags2] = xcorr(xx1,xx3,'coeff');
[c_ww3,lags3] = xcorr(xx1,xx4,'coeff');
[c_ww4,lags4] = xcorr(xx1,xx5,'coeff');
[c_ww5,lags5] = xcorr(xx1,xx6,'coeff');
[c_ww6,lags6] = xcorr(xx1,xx7,'coeff');

%Plot figures

plot(lags1,c_ww1,'k');
hold on
plot(lags2,c_ww2,'y');
hold on
plot(lags3,c_ww3,'b');
hold on
plot(lags4,c_ww4,'g');
hold on
plot(lags5,c_ww5,'c');
hold on
plot(lags6,c_ww6,'m');
hold on

xlabel('Distance (m)', 'FontSize',30);
ylabel('Cross Correlation ', 'FontSize',30)
set(gca, 'FontSize',26)

axis([-100 100 0.6 1])

hleg1 =
legend('\fontsize{15}Xcorr(vt,vl1)', '\fontsize{15}Xcorr(vt,vl2)', '\fontsize{15}Xcorr(vt,vl3)', '\fontsize{15}Xcorr(vt,vl4)', '\fontsize{15}Xcorr(vt,vl5)', '\fontsize{15}Xcorr(vt,vl6)');
```


C.2 Code for Power Spectrum

```
%Sampling rate is 50

Fs=1/0.02;

%Calculate power spectrum density of wind speed

[Pss_1,f1]=pwelch(xx1,[],[],length(xx1),Fs,'oneside');
loglog(2*pi*f1(2:end),Pss_1(2:end),'color','k')

hold on

[Pss_1,f1]=pwelch(xx2,[],[],length(xx2),Fs,'oneside');
loglog(2*pi*f1(2:end),Pss_1(2:end),'color','y')

hold on

[Pss_1,f1]=pwelch(xx3,[],[],length(xx3),Fs,'oneside');
loglog(2*pi*f1(2:end),Pss_1(2:end),'color','r')

hold on

[Pss_1,f1]=pwelch(xx4,[],[],length(xx4),Fs,'oneside');
loglog(2*pi*f1(2:end),Pss_1(2:end),'color','g')

hold on

[Pss_1,f1]=pwelch(xx5,[],[],length(xx5),Fs,'oneside');
loglog(2*pi*f1(2:end),Pss_1(2:end),'color','b')

hold on

[Pss_1,f1]=pwelch(xx6,[],[],length(xx6),Fs,'oneside');
loglog(2*pi*f1(2:end),Pss_1(2:end),'color','m')

xlabel('Frequency (Hz) ','FontSize',30);
ylabel('Spectrum (m/s)^2/Hz ','FontSize',30)
set(gca,'FontSize',26)
```

Appendix C. Matlab Code for the Project

```
hleg1=legend('\fontsize{18}v11', '\fontsize{18}v12', '\font  
size{18}v13', '\fontsize{18}v14', '\fontsize{18}v15', '\font  
size{18}v16');
```

C.3 Code for Cross Power Spectrum

```
%Sampling rate is 50

Fs=1/0.02;

%Calculate cross spectrum of xx1 and xx2
[Pss_1, f1]=cpsd(xx1,xx2, [], [], length(xx1), Fs, 'oneside');
loglog(2*pi*f1(2:end), Pss_1(2:end), 'k')

hold on

%Calculate cross spectrum of xx1 and xx3
[Pss_1, f1]=cpsd(xx1,xx3, [], [], length(xx1), Fs, 'oneside');
loglog(2*pi*f1(2:end), Pss_1(2:end), 'y')

hold on

%Calculate cross spectrum of xx1 and xx4

[Pss_1, f1]=cpsd(xx1,xx4, [], [], length(xx1), Fs, 'oneside');
loglog(2*pi*f1(2:end), Pss_1(2:end), 'r')

hold on

%Calculate cross spectrum of xx1 and xx5

[Pss_1, f1]=cpsd(xx1,xx5, [], [], length(xx1), Fs, 'oneside');
loglog(2*pi*f1(2:end), Pss_1(2:end), 'g')

hold on

%Calculate cross spectrum of xx1 and xx6

[Pss_1, f1]=cpsd(xx1,xx6, [], [], length(xx1), Fs, 'oneside');
loglog(2*pi*f1(2:end), Pss_1(2:end), 'b')

xlabel('Frequency (Hz)', 'FontSize', 30);
ylabel('Cross Spectrum((m/s)^2/Hz)', 'FontSize', 30)
set(gca, 'FontSize', 26)
```

Appendix C. Matlab Code for the Project

```
hleg1=legend('\fontsize{18}S(vt,vl1)', '\fontsize{18}S(vt,  
vl2)', '\fontsize{18}S(vt,vl3)', '\fontsize{18}S(vt,vl4)', '  
\fontsize{18}S(vt,vl5)', '\fontsize{18}S(vt,vl6)');
```

C.4 Wind Turbine Control System Simulink Model

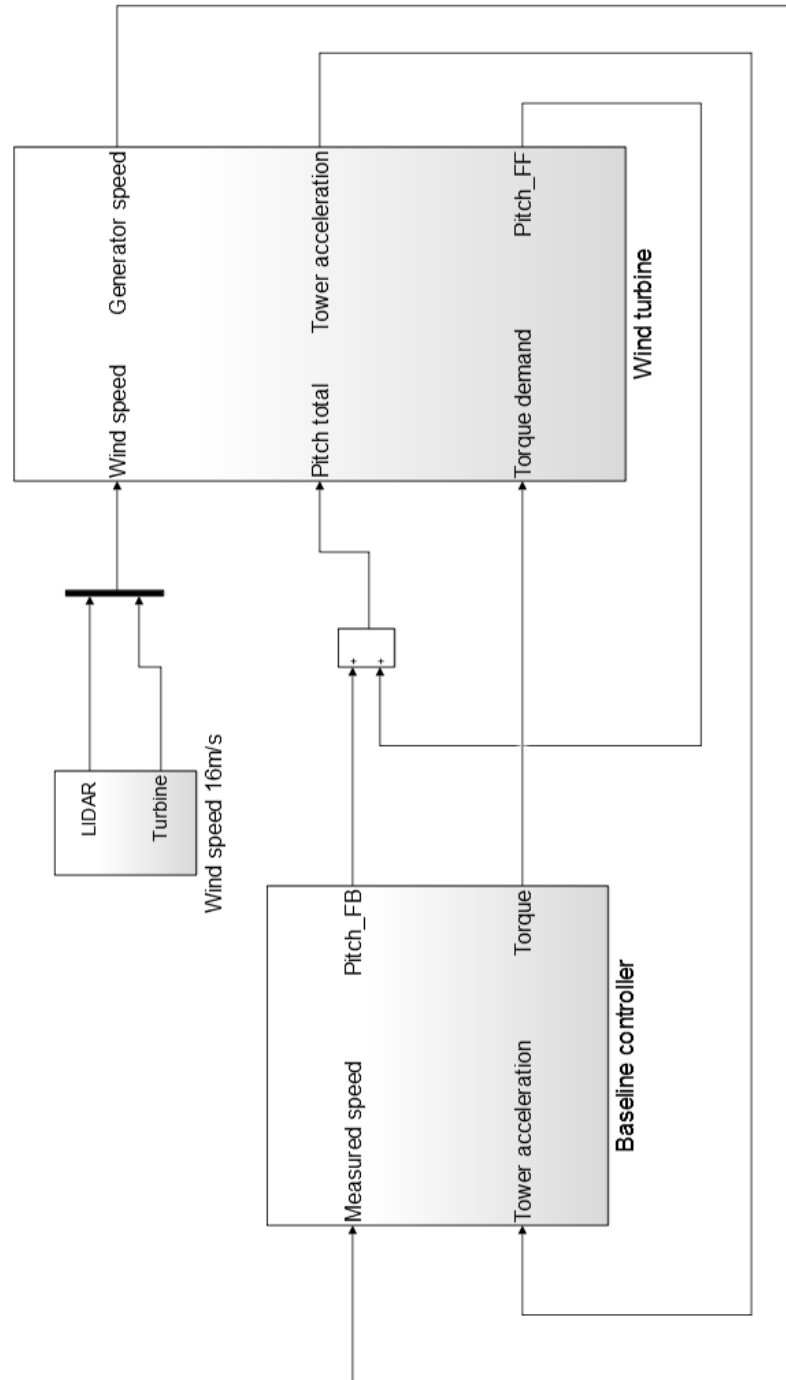


Figure C.1: Simulink model of the whole control system

Appendix C. Matlab Code for the Project

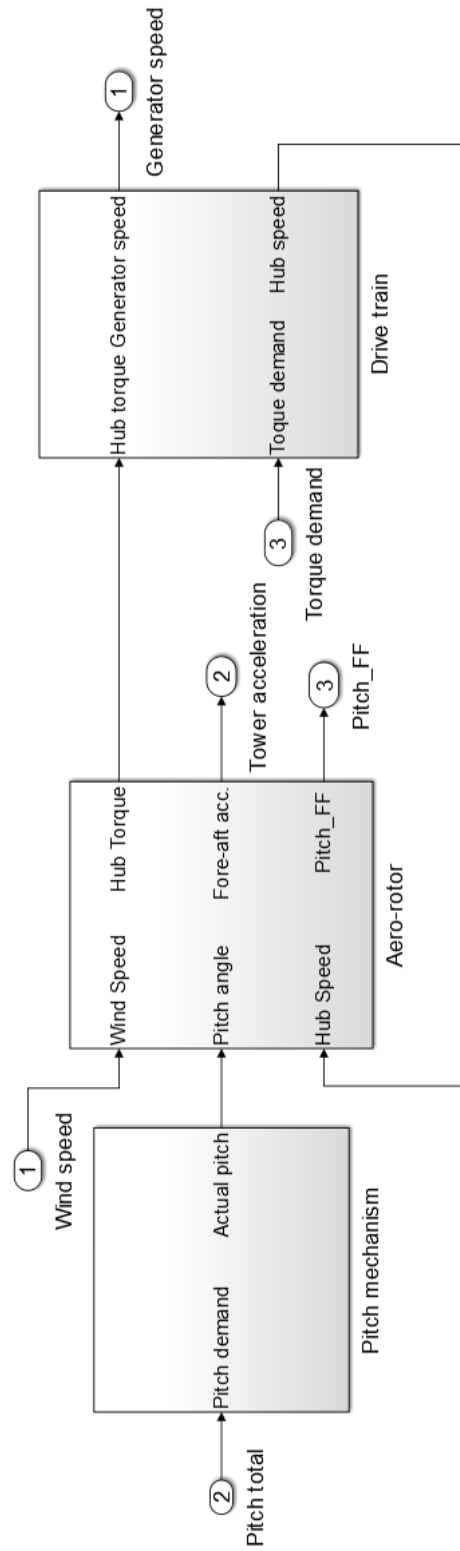


Figure C.2: Wind turbine Simulink model

Appendix C. Matlab Code for the Project

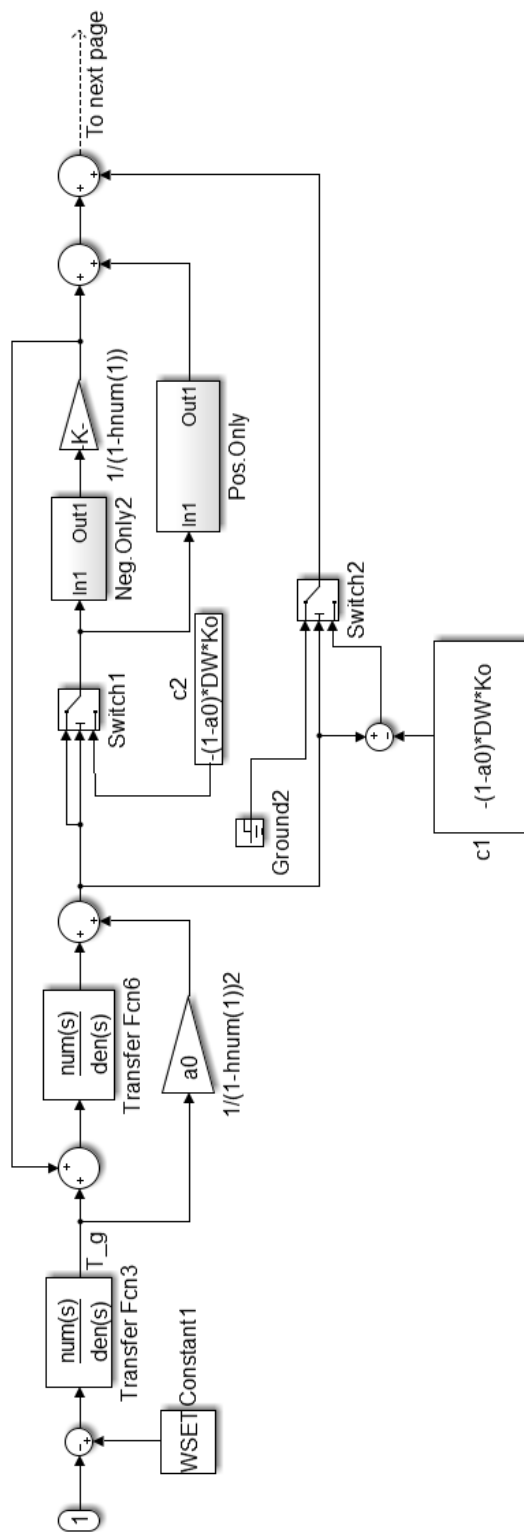


Figure C.3: Part 1 of the baseline controller

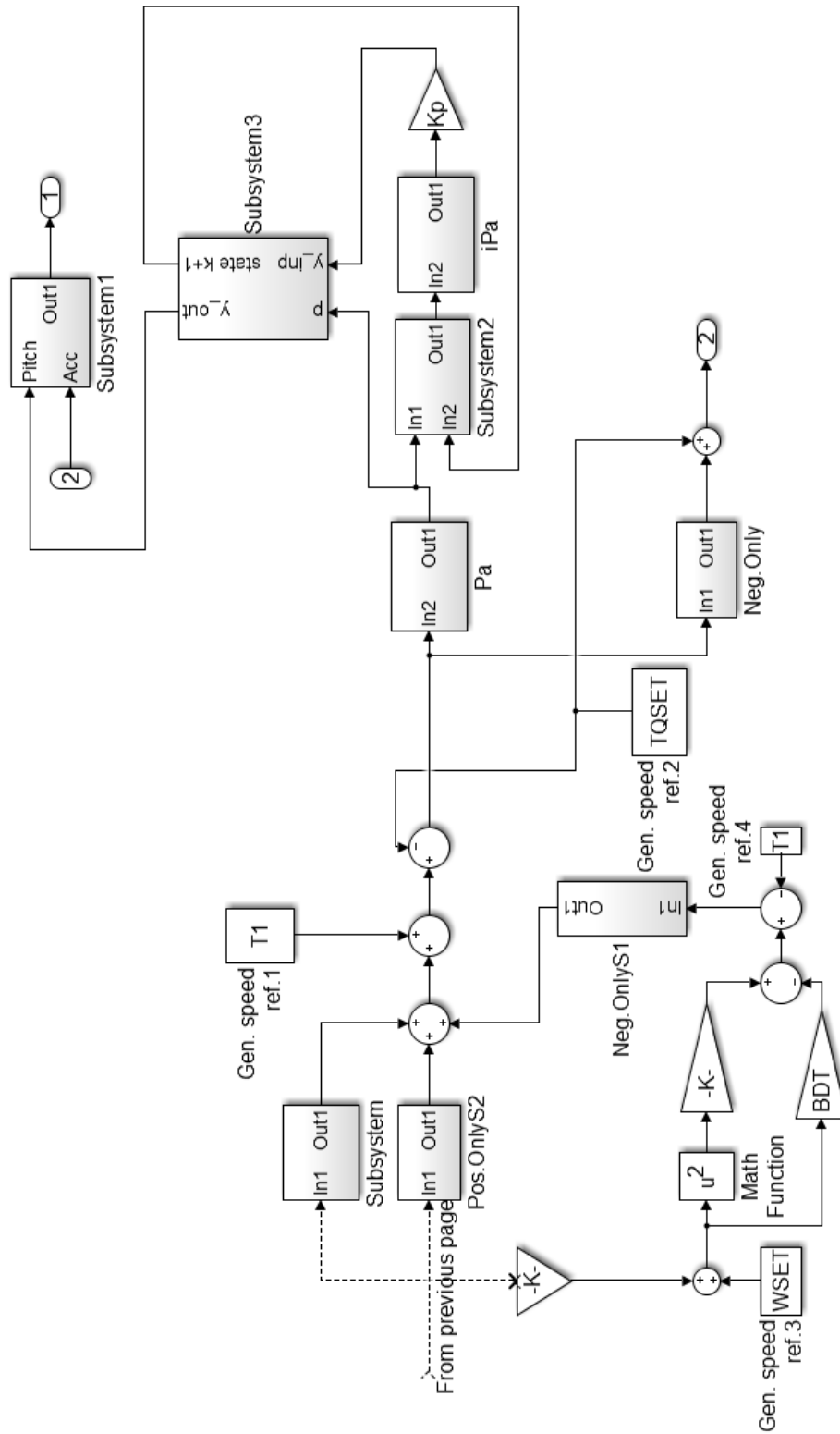


Figure C.4: Part 2 of the baseline controller

Appendix C. Matlab Code for the Project

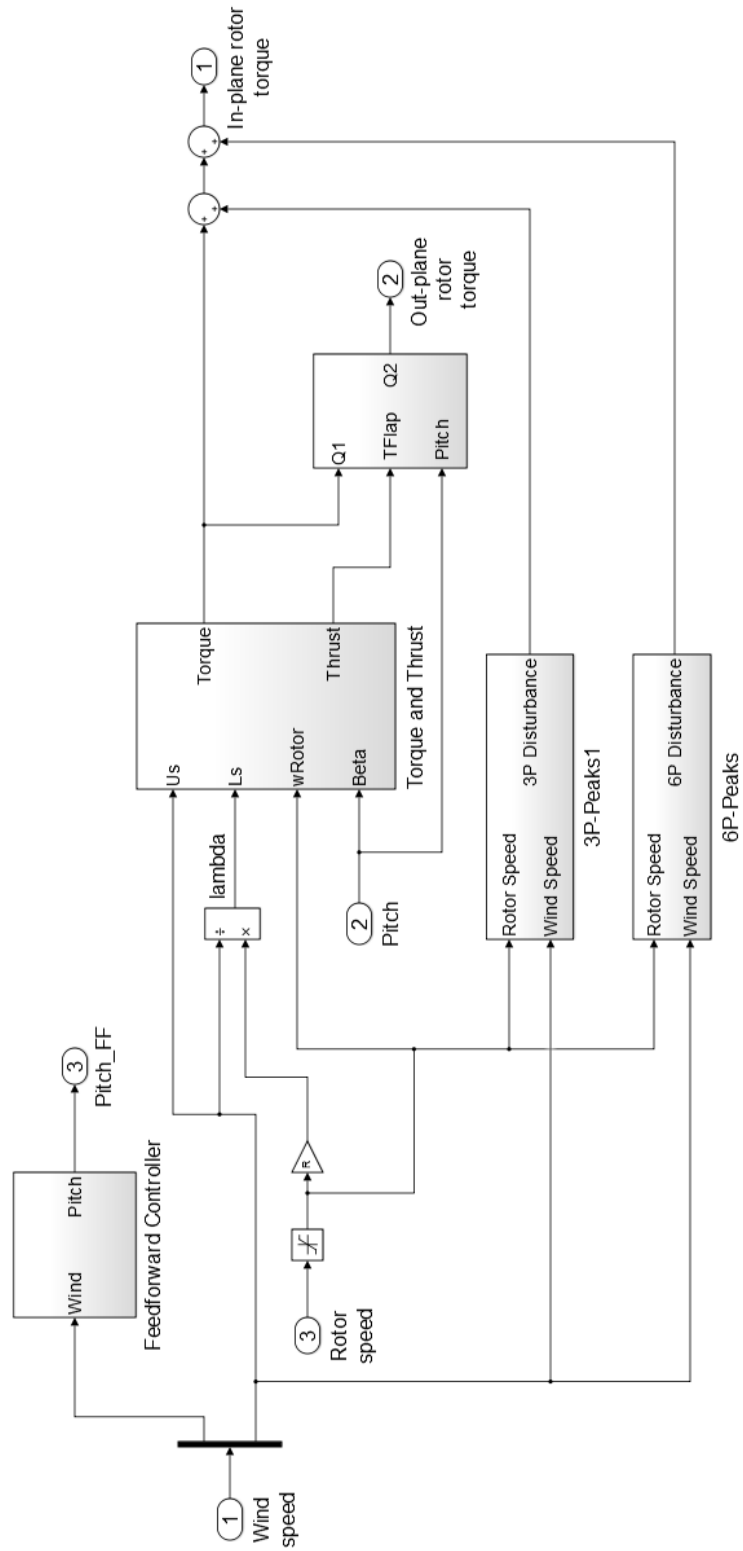


Figure C.5: Feedforward control loop